



HAL
open science

Safer-by-Design Fluorescent Nanocrystals: Metal Halide Perovskites vs Semiconductor Quantum Dots

Dmitry Aldakov, Peter Reiss

► **To cite this version:**

Dmitry Aldakov, Peter Reiss. Safer-by-Design Fluorescent Nanocrystals: Metal Halide Perovskites vs Semiconductor Quantum Dots. *Journal of Physical Chemistry C*, 2019, 10.1021/acs.jpcc.8b12228 . hal-02373685

HAL Id: hal-02373685

<https://hal.science/hal-02373685v1>

Submitted on 15 Dec 2020

HAL is a multi-disciplinary open access archive for the deposit and dissemination of scientific research documents, whether they are published or not. The documents may come from teaching and research institutions in France or abroad, or from public or private research centers.

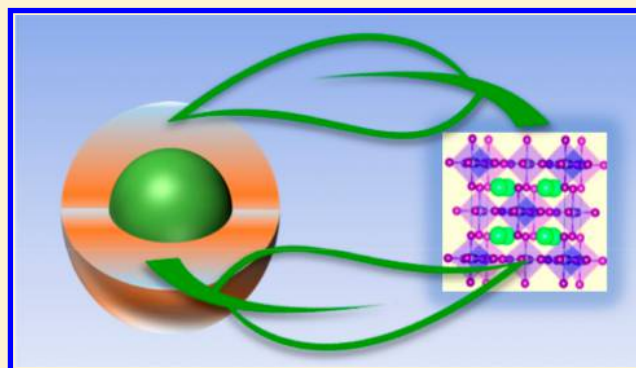
L'archive ouverte pluridisciplinaire **HAL**, est destinée au dépôt et à la diffusion de documents scientifiques de niveau recherche, publiés ou non, émanant des établissements d'enseignement et de recherche français ou étrangers, des laboratoires publics ou privés.

Safer-by-Design Fluorescent Nanocrystals: Metal Halide Perovskites vs Semiconductor Quantum Dots

Dmitry Aldakov*¹ and Peter Reiss*²

University Grenoble-Alpes, CNRS, CEA, INAC/SyMMES/STEP, 38000 Grenoble, France

ABSTRACT: Despite the young age of the research field, substantial progress has been made in the study of metal halide perovskite nanocrystals (HPNCs). Just as their thin-film counterparts are used for light absorption in solar cells, they are on the way to revolutionizing research on novel chromophores for light emission applications. Exciting physics arising from their peculiar structural, electronic, and excitonic properties are being discovered with breathtaking speed. Many things we have learned from the study of conventional semiconductor quantum dots (CSQDs) of II–VI (e.g., CdSe), IV–VI (e.g., PbS), and III–V (e.g., InP) compounds have to be thought over, as HPNCs behave differently. This Feature Article compares both families of nanocrystals and then focuses on approaches for substituting toxic heavy metals without sacrificing the unique optical properties as well as on surface coating strategies for enhancing the long-term stability.



1. INTRODUCTION

In the early 1980s the quest for novel photocatalysts, fueled by the oil crisis in the preceding decade, led to the discovery of semiconductor quantum dots. Pioneering works by Efros, Brus, and Henglein showed both experimentally and theoretically that the reduction of size of semiconductor particles (e.g., CdS) down to the nanometer range induces a significant change in their band gap energy.^{1–3} The underlying quantum confinement effect, occurring when the nanocrystal size is (significantly) smaller than twice the exciton Bohr radius of the semiconductor material (Table 1), leads to an increase, scaling with $1/r^2$, of the band gap energy.⁴ It also gives rise to the appearance of discrete energy levels at the place of continuous valence and conduction energy bands. In the same period Ekimov as well as Itoh and co-workers observed quantum confinement in small CuCl crystallites embedded in a glass or a NaCl matrix.^{5–7} However, although being the first example of quantum-confined metal halide nanocrystals, the large band gap energy (3.2 eV) and low exciton Bohr radius (0.7 nm) due to strong Coulomb interaction in CuCl have limited the research interest in this material. In contrast, nanocrystals of II–VI semiconductors, in particular, of cadmium chalcogenides, have seen tremendous development. Chemical synthesis methods giving access to precisely controlled nanocrystal size and low size distribution⁸ as well as efficient strategies for surface passivation via growth of a shell of a larger band gap material^{9,10} paved the way for the in-depth investigation of the photophysical properties of this new class of materials. The most outstanding property of what will be termed in the following *conventional semiconductor quantum dots* (CSQDs) is their fluorescence: not only can it be finely tuned with the nanocrystal size, but also

the emission spectrum is narrow and the room temperature quantum yield is high, reaching nearly unity upon proper surface passivation.¹¹ These features make CSQDs very interesting emitters for a multitude of applications such as LEDs, luminescent solar concentrators, biological imaging/detection, and so on.^{12,13} One important aspect when it comes to real-life applications is the impact of nanoparticles on human health and environment. This issue concerns the whole life cycle of QDs, from their synthesis over their practical use to their disposal and eventual disintegration. The question of toxicity of a nanocrystal is a complex one: toxicity for living organisms can arise from the nanodimensions, e.g., induced by photocatalytic activity triggered by the very high surface-to-volume ratio, as well as from the chemical elements and molecules constituting the inorganic core and the organic ligand shell of QDs.¹⁴ Moreover, after their translocation through the primary target organs (skin, intestine, lung), nanocrystals in a living organism may undergo chemical modifications, which can lead to the release of toxic ions or the formation of harmful degradation products. All these effects are strongly dependent on the size, composition, and surface state of the nanocrystals, and therefore the establishment of systematic toxicity studies enabling a more general classification of CSQDs is hampered. Health risks related to chemical substances in general and to nanoparticles in particular are defined as a combination of hazard and exposure. Therefore, a key principle to effectively limit the risk related to nanocrystals is the safer-by-design approach,

Received: December 19, 2018

Revised: January 14, 2019

Published: January 18, 2019

Table 1. Materials' Parameters of Selected Compounds Used in CSQDs and HPNCs

compound	exciton Bohr radius (nm)	m_e^* , m_h^* (electron mass)	bulk band gap (eV)	room-temperature crystal structure
CdSe	5.0	0.13, 0.45	1.74	hexagonal (wurtzite)
CdTe	4.6	0.10, 0.48	1.45	cubic (zinc blende)
ZnO	2.4	0.28, 0.54	3.20	hexagonal (wurtzite)
ZnSe	3.1	0.21, 0.60	2.82	cubic (zinc blende)
ZnTe	3.9	0.2, 0.2	2.39	cubic (zinc blende)
PbS	23.5	0.08/0.105 0.075/0.105 ^a	0.35	cubic (halite)
PbSe	66	0.04/0.07, 0.034/0.068 ^a	0.27	cubic (halite)
InP	9.6	0.077, 0.64	1.35	cubic (zinc blende)
InAs	36.2	0.023, 0.30	0.36	cubic (zinc blende)
InSb	64.9	0.015, 0.39	0.17	cubic (zinc blende)
CuInS ₂	4.1	0.16, 1.30	1.45–1.53	tetragonal (chalcopyrite)
CuInSe ₂	10.6	0.09, 0.73	1.04–1.07	tetragonal (chalcopyrite)
AgInS ₂	5.5	0.15, 1.36	1.83–1.87	orthorhombic
CsPbCl ₃	5	0.20	2.96	cubic
CsPbBr ₃	7	0.15, 0.14	2.34	orthorhombic
CsPbI ₃	12	0.11	1.72	orthorhombic ^b
MAPbBr ₃	2.0	0.13	2.29	pseudocubic
FAPbI ₃	6.35	0.095	1.52	pseudocubic ^b

^aThe two values indicate the transverse and longitudinal effective masses at 4 K. ^bMetastable at room temperature.

which reduces the toxicity hazard by replacing QDs containing toxic heavy metals by alternative materials. This is a very active field of research,^{14,15} which will be discussed in the main part of this article.

In contrast to CSQDs, metal halide perovskite nanocrystals (HPNCs) are a newly emerging research field, with the very first paper dating from 2014. Initially, organic–inorganic hybrid perovskite NCs such as methylammonium lead bromide (MAPbBr₃) were developed by Galian and Pérez-Prieto and later by Zhong and co-workers.^{16–18} The interest in this family of semiconductors, in particular MAPbI₃ (“MAPI”), arose from their very successful incorporation as light harvesters in solar cells,^{19,20} which was totally unexpected for a polycrystalline material with a high defect density. In addition to hybrid HPNCs, fully inorganic lead halide perovskite nanocrystals such as CsPbBr₃ have first been reported by Kovalenko and co-workers.²¹ In both cases, the most intriguing feature is their very strong photoluminescence (PL), reaching quantum yields close to unity with no necessity for surface passivation other than by pristine ligand coverage. Another striking contrast to CSQDs is that color tuning is most easily achieved not by size variation but via solution-phase anion exchange, with a reduction of the band gap energy in the order Cl > Br > I.^{22,23} On the other hand, HPNCs share one important feature with initially developed CSQDs: as in the case of Cd-based QDs once again a toxic heavy metal ion (Pb) plays a central role in governing the optical and electronic properties. In the following, we first confront the specific properties of both families of nanocrystals. Next, we give a brief overview of the strategies developed toward safer-by-design toxic-heavy-metal-free CSQDs and HPNCs. Finally, we highlight the challenges and possible future directions of this research field.

2. OPTICAL PROPERTIES OF CSQDs AND HPNCs

2.1. Excitons. As mentioned above, hybrid perovskites like MAPI are very efficient active materials for light absorption in solar cells. Apart from their appropriate band gap of around 1.6 eV and their high absorption coefficient, one of their key features for photovoltaic (PV) applications is the fast

rotational dynamics of the dipolar methylammonium cation within the cuboctahedral cages in the 3D structure formed by corner-sharing PbI₆ octahedra.²⁴ This rotation leads to structural and potential fluctuations and a giant photoinduced dielectric constant.²⁵ As a result, the Coulomb interaction between charge carriers is effectively screened, which contributes to the reduction of the exciton binding energy $E_{b,exc}$ (16 meV at low temperature, a few meV at room temperature).²⁶ By consequence, free carriers (and not excitons) play the major role in the photovoltaic performances of polycrystalline perovskite thin films. Radiative recombination is a minor deexcitation process, and accordingly, PL studies performed on polycrystalline MAPbBr₃ showed only weak emission with a quantum yield (QY) on the order of 1%.²⁷ However, when reducing the crystallite size to micro- or nanocrystals, a strong enhancement of the QY to 80% is observed, attributed to the predominant presence of excitons and efficient passivation of surface trap states by the used organic ligands. Obviously, when reducing the size to the nanometer range the exciton binding energy increases because of the increased spatial overlap of the electron and the hole (quantum confinement) but also due to the increase of the contribution of dielectric confinement. The latter is the consequence of the difference of the dielectric constants of the inorganic nanocrystal core and its surrounding medium (including surface ligands). The increase of dielectric confinement in the case of smaller crystallites is representative of the larger opportunity for the electric force lines to penetrate into the surrounding medium. An exciton binding energy ($E_{b,exc}$) value of 320 meV has been determined by X-ray photoelectron spectroscopy for 8 nm CsPbBr₃ nanocrystals.²⁸ Just like hybrid halide perovskites, their fully inorganic counterparts also display low exciton binding energies in the bulk, as determined by magneto-optical studies on single crystals:²⁹ 33 meV for CsPbBr₃ and 15 meV for CsPbI₃; for CsPbCl₃, a value of 75 meV has been calculated using the effective mass model. As expected, in both the hybrid and inorganic perovskites the $E_{b,exc}$ values increase with the band gap energy of the compound, i.e., $E_b(\text{APbX}_3)$: Cl > Br > I (A = MA, Cs). Due to the absence of phase transitions and

structural fluctuations when replacing the dipolar methylammonium rotor by Cs ions, $E_{b,exc}$ is essentially temperature-independent in all-inorganic HPNCs. Even though experimentally determined values are lacking to date, it can be predicted that, as with hybrid perovskites, $E_{b,exc}$ significantly increases when going from the bulk to nanocrystals due to the effects of quantum and dielectric confinement. For comparison, in the case of small-sized CSQDs, exciton binding energies of around 100 meV (CdSe) and 1000 meV (CdS), being 1 order of magnitude larger than for the bulk materials, have been determined using photoelectron spectroscopy.³⁰

In conclusion, reducing the size of hybrid or all-inorganic halide perovskites to the nanoscale and introducing surface ligands to stabilize them as colloids lead to an increase of the exciton binding energy to values comparable to those characteristic of CSQDs. Even in the weak confinement regime excitons formed in HPNCs are stable at room temperature ($E_{b,exc} > 26$ meV at 300 K),²⁷ which is highly beneficial for light-emission applications.

2.2. Quantum Confinement and Photoluminescence Properties. Size control is the main method for adjusting the fluorescence wavelength of CSQDs via the quantum confinement effect. The downside of exploiting the size-dependent band gap energy is a broadening of the emission line width and hence reduced color purity due to the size distribution in colloidal nanocrystal samples. The narrowest line widths obtained with CdSe QDs emitting in the visible range are on the order of 20 nm, while with the Cd-free alternative InP QDs it is challenging to achieve values <40 nm. At the same time, due to the decrease of the confinement energy and differences in the electron and hole effective masses, the fluorescence efficiency of CSQDs is generally decaying significantly when moving from the strong to the weak confinement regime, i.e., by increasing the size close to twice the exciton Bohr radius. The situation is completely different in HPNCs, as there, even for weakly or nonconfined nanocrystals, excellent fluorescence QYs can be obtained. In this case, a combination of high oscillator strength of the radiative transition and of efficient passivation of surface traps/absence of deep traps (vide infra) is supposed to be at the origin of this behavior.²⁷

As outlined above, CSQDs exhibit the best PLQY in the strong confinement regime. On the other hand, due to the large surface-to-volume ratio and the related high density of trap states, efficient surface passivation strategies are required, such as shell growth of larger band gap semiconductors. In addition to size distribution induced spectral broadening observed in colloidal solutions of CSQDs, other drawbacks associated with the strong confinement regime are (radiative) reabsorption processes and (nonradiative) Förster resonance energy transfer (FRET) from the smaller dots to the larger ones in the ensemble.³¹ In close-packed solid-state QD films these effects become particularly visible through the bathochromic shift and line narrowing of the emission peak compared to the colloidal sample, generally accompanied by a decrease of the PL intensity (cf. Figure 1a).³² To the contrary, weakly confined 11 nm CsPbBr₃ HPNCs exhibit quasi-identical emission properties in the colloidal and in the solid state (cf. Figure 1b). In addition, postdeposition surface treatment with lead halides (e.g., PbBr₂) can further improve the PLQY of HPNC thin films up to near unity.³³ By replacing the Cs⁺ cation by formamidinium (FA⁺) perovskite NCs can be achieved with high stability and PL tunability as a

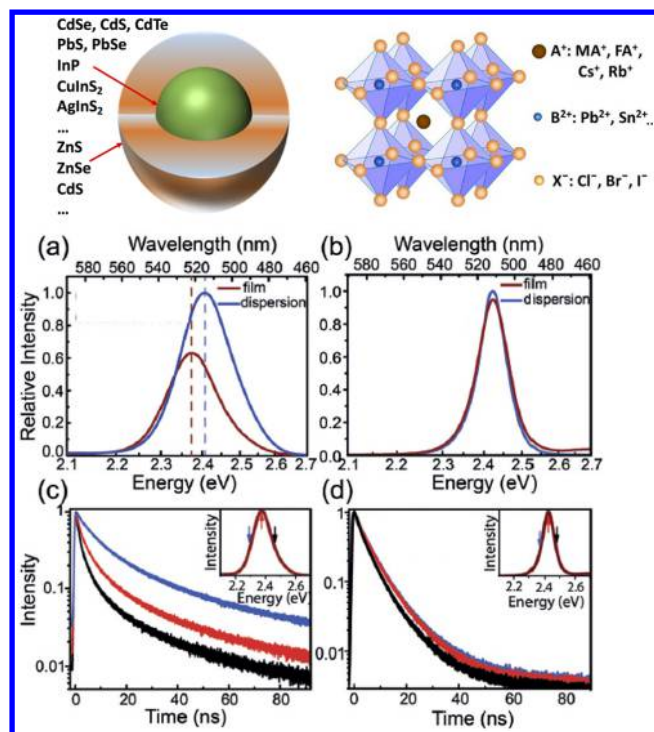


Figure 1. Top row: schemes showing the structure of a core/shell CSQD and the basic crystal structure found in HPNCs. (a–d) Comparison of CdSe/CdS-ZnS core/shell QDs (left column) and CsPbBr₃ HPNCs (right column). (a/b) Steady-state PL spectra in colloidal solution and on thin films, normalized with absorbance at the excitation wavelength (400 nm). (c/d) PL decay curves at different emission wavelengths. Adapted from ref 41. Reproduced with permission from Wiley-VCH Verlag GmbH & Co. KGaA 2015.

function of size (related to quantum confinement).^{34,35} Looking at the PL decay dynamics of CdSe/CdS-ZnS core/shell QDs, a faster decay at higher emission energies is observed, due to the increasing importance of additional deexcitation channels associated with FRET (cf. Figure 1c). Such a dependence is nearly absent in the case of HPNCs, suggesting a very limited contribution of FRET-related processes (cf. Figure 1d). The PL decay times for CsPbBr₃ were fitted with two exponentials, yielding in this case radiative decay times of 3 and 8 ns. These values are shorter than those observed with CSQDs, generally in the range of some tens of ns for binary to some hundreds of ns for multinary systems. Moving from ensemble to single-particle measurements enables probing the effects of trap states on carrier dynamics by analyzing PL fluctuations with time. In CSQDs, fluorescence intermittency (“blinking”) observed in single-particle spectroscopy, i.e., periodic switching between “on” and “off” states following power law statistics (or crossover from power law to exponential behavior), has been studied for two decades.³⁶ Several hypotheses concerning the underlying mechanisms have been formulated, which have in common that they imply charge carrier trapping at defects in the nanocrystal, at the surface, or external to the nanocrystal. Charge carrier trapping negatively affects both the PLQY and charge transport properties. It leads to ionized nanocrystals, and subsequently generated electron–hole pairs recombine via fast nonradiative Auger processes. One efficient way to strongly reduce blinking in CSQDs is the growth of so-called “giant” shells, which implies the use of materials of low lattice

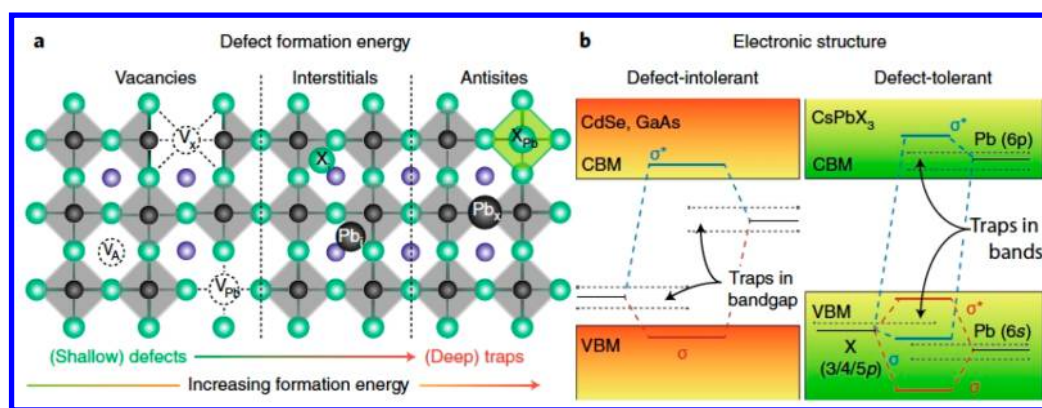


Figure 2. (a) Typical point defects in lead halide perovskites in the order of increasing formation energy/decreasing probability of occurrence. (b) Schematic representation of the band structure of typical defect-intolerant semiconductors (CdSe, GaAs) and of metal halide perovskites. In the latter case, the VBM exhibits antibonding character. Reproduced with permission from ref 47. Copyright 2018 Springer Nature Publishing AG.

mismatch, e.g., CdSe and CdS.³⁷ Recently, suppressed blinking combined with near unity PLQY, monoexponential decay (20 ns), and ensemble PL line widths down to 19 nm (53 meV) were achieved with CdSe/CdS QDs having intermediate shell thicknesses (3–8 monolayers) by optimizing the synthesis conditions, in particular the organic ligands used.³⁸ Blinking is also observed in HPNCs, even though the measurement conditions need to be adapted in order to avoid their rapid photobleaching.³⁹ These initial studies indicate that HPNCs tend toward longer “on” durations than CSQDs, that the blinking kinetics are excitation intensity dependent, and that a diffusion-controlled electron transfer mechanism (DCET) plays a more important role than Auger ionization. More recent works reveal two distinct types of PL fluctuations:⁴⁰ (i) Flickering (continuous distribution of PL intensity as a function of time) is caused by excess surface trap states and can be reduced or suppressed by postsynthetic surface treatment (e.g., with alkylthiols). These traps are attributed to undercoordinated lead atoms, which act as short-lived, shallow electron traps. (ii) Blinking, resulting from trion formation due to the presence of longer-lived traps originating from intrinsic defects. Importantly, both types of defects exhibit dynamic nature induced by the diffusion of surface ligands and the mobility of the ions constituting HPNCs, leading to dispersive emission kinetics.

3. SPECIFICITIES OF Cd- AND Pb-CONTAINING NCS FAVORING OUTSTANDING OPTOELECTRONIC PROPERTIES

The initial large interest in Cd-based CSQDs, in particular, CdSe and CdTe, was motivated by the fact that their bulk band gap allows tuning their PL throughout the visible spectral range by changing their size (Table 1). Another key factor was the development of very efficient synthesis methods giving access to samples with size distributions <10% without size fractionation.⁸ Finally, the growth of inorganic shells (e.g., ZnS, ZnSe, CdS) resulted in highly emissive, photostable QDs of high interest for both fundamental and applied science.¹⁰ This family of QDs was complemented by lead chalcogenide nanocrystals, which gave access to the longer wavelengths of absorption and emission, in particular in the 1–2 μm range.⁴² Interestingly, nonoxidized Pb-chalcogenide QDs can exhibit bright luminescence without surface modification via shell growth, which suggests a certain defect tolerance (see below).

In terms of synthesis, Cd- and Pb-chalcogenide QDs benefit from an intermediate fractional ionic character of bonding;¹⁴ i.e., they are less covalent than III–V semiconductors and less ionic than HPNCs. In the former case, harsh reaction conditions and highly reactive precursors are required, making it difficult to effectively separate nucleation and growth, which is a prerequisite for obtaining narrow size distributions.¹⁴ In the latter case, perovskite nanocrystals simply dissolve when brought into contact with polar solvents (including water); therefore, substantial efforts are currently made for enhancing their chemical stability.

To understand the outstanding photophysical properties of HPNCs their electronic structure has to be considered. In particular, their bright emission without surface passivation using an epitaxial inorganic shell demonstrates that no deep trap levels (“killer defects”) are formed despite disruption of the crystalline lattice at the nanocrystal surface. In the form of polycrystalline thin films, lead halide perovskites exhibit excellent properties as solar cell active material, despite the presence of a much higher density of defects than conventional photovoltaic materials like silicon. One factor contributing strongly to this behavior is the high dielectric constant in halide perovskites and the resulting effective screening of electrostatic perturbations. Furthermore, in lead halide perovskites the occurrence of defects leading to deep trap states (e.g., interstitial atoms or antisite defects) is impeded by their much higher formation energy (Figure 2a).⁴³ Another important feature is their peculiar band structure as revealed by first-principles calculations:^{44,45} while the A-site cations (Cs⁺, MA⁺, etc.) do not contribute to the band edge states, the valence band maximum (VBM) results from the strong antibonding interaction between Pb 6s and halide 3/4/5p orbitals, shifting it above the latter (cf. Figure 2b). The antibonding conduction band minimum (CBM) has predominant Pb 6p character and exhibits strong influence of relativistic spin–orbit coupling effects.⁴⁶ As a result, structural defects arising, for example, from A-site or X-site vacancies in ABX₃ lead to defects that are located within the CB or VB, respectively, or to shallow defects.⁵⁰

This implies that both thin films and HPNCs preserve a “clean” band gap, which means that the defects possess mostly benign character and are not optically and electrically active.⁴⁸ Another unique property of the halide perovskites is their defect self-healing, in other words, the fact that defects

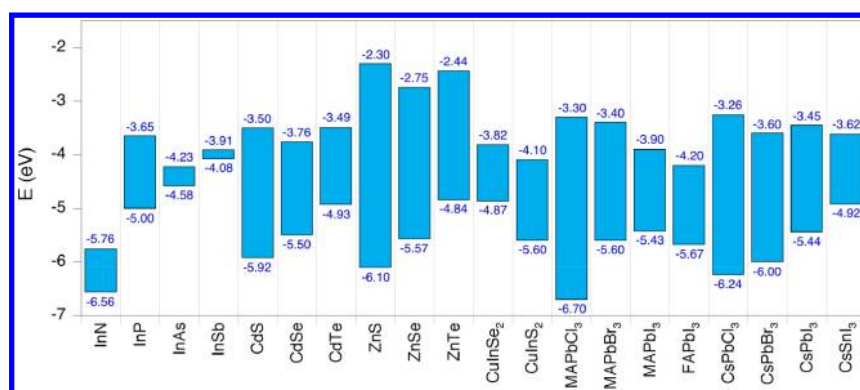


Figure 3. Energy levels (valence band maximum, VBM/conduction band minimum, CBM) of selected CSQDs (left) and HPNCs (right).

appearing during preparation or device operation can disappear spontaneously.⁴⁹ Therefore, this class of materials is termed “defect tolerant”, and this property is of crucial importance for all optoelectronic applications.⁵⁰ To the contrary, in defect-intolerant semiconductors (e.g., CdSe, GaAs, Si, etc.) the band gap is formed between bonding and antibonding orbitals, which leads to the location of all defect levels as either shallow or deep traps within the band gap.

Summarizing, lead halide perovskite nanocrystals exhibit—in contrast to CSQDs—a pronounced defect tolerance due to their intrinsic electronic structure and the high formation energy of defects leading to deep trap states, which would be detrimental for photoluminescence and electronic transport. In CSQDs, the growth of an epitaxial inorganic shell is generally required to passivate trap states and increase the PL intensity. It remains to be demonstrated whether the advantageous features of Pb-based perovskite nanocrystals can be translated to Pb-free compositions.

4. GENERAL STRATEGIES FOR REPLACING TOXIC HEAVY METALS IN NANOCRYSTALS

In CSQDs the bulk band gap of the used semiconductor material is the first parameter to consider; as quantum confinement leads to its widening, the initial band gap should be lower than 2 eV when size-tunable emission in the visible range is targeted. This requirement is less stringent in the case of weakly or nonconfined HPNCs where the band gap is mainly adjusted by the composition. As visible in Figure 3, within the CsPbX₃ and MAPbX₃ families, a change of the halide more strongly affects the VBM position than the CBM position. For CSQDs it has been shown that the absolute VBM and CBM positions can be shifted by as much as 2 eV through solution-phase surface ligand exchange.⁵¹ The knowledge of these levels is, together with the crystallographic parameters, of fundamental importance for the design of core/shell structures.¹⁰

Below we present the main strategies for developing safer-by-design lead-free or lead-deficient HPNCs as well as Cd-free CSQDs.

4.1. Isovalent Atom Replacement. For the isovalent replacement of lead in HPNCs, the choice of alternative divalent metal ions is first guided by geometrical models. The latter have been established for bulk materials to predict the formability of the 3D ABX₃ perovskite structure, which plays the central role for realizing the unique optoelectronic properties discussed above. These models are based on two empirical parameters, the Goldschmidt tolerance factor t and

the octahedral factor μ .⁵² The former can be calculated using the ionic radii of the three implied elements (eq 1), while the latter simply displays the radius ratio of the B-site cation over the halide anion (eq 2); in other words, it reflects the stability of the basic BX₆ octahedral building unit.

$$t = (r_A + r_X) / \sqrt{2} (r_B + r_X) \quad (1)$$

$$\mu = r_B / r_X \quad (2)$$

By analyzing 186 complex halide compounds, Li and co-workers found that 3D ABX₃ perovskite formability could be predicted with 96% accuracy when the following boundary conditions for t and μ were chosen:⁵² $0.813 < t < 1.107$ and $0.442 < \mu < 0.895$. Nonetheless, it should be kept in mind that the two factors reflect necessary but not sufficient conditions for perovskite formability.

One way to relieve the restrictions imposed by these geometric boundaries is changing perovskite dimensionality. This property should not be confused with the crystal habit or morphology. The HPNCs discussed so far exhibit 3D dimensionality due to their 3D corner-sharing PbX₆ octahedra framework while being considered—like quantum dots—as 0D materials. The cuboctahedral cavity enclosed by neighboring octahedra can only accommodate small A-site cations (e.g., Cs⁺, MA⁺, FA⁺). Going to larger cations typically leads to the disruption of the 3D network and decrease of the perovskite dimensionality by “slicing” the 3D structure into 2D slabs. A widely studied family of 2D perovskites obtained by cutting along the $\langle 100 \rangle$ direction of the parent compound has the general formula (RNH₃)₂A_{*n*-1}BX_{3*n*+1} (n : integer) with R being a (bulkier) primary amine or aromatic alkylammonium cation inducing the spacing between the perovskite layers and A a smaller cation (e.g., methylammonium). Their structure is analogous to that of 2D oxide perovskites studied by Ruddlesden and Popper,⁵³ and their dimensionality can be tuned in principle from 2D to 3D by changing n from 1 to infinity.⁵⁴ As the perovskite sheets are separated by the organic moieties of the alkylammonium cations, the structure can be considered as a multilayer quantum well. Quantum confinement occurs along the stacking direction $\langle 100 \rangle$ and is more pronounced the smaller the number of n . One important feature of the 2D perovskites is their enhanced environmental stability as compared to their 3D counterparts.⁵⁵

Total Precursor Replacement. The simplest concept to limit the toxicity of CSQDs related to the presence of heavy metal elements is to replace them by isovalent atoms having similar properties in terms of size and chemical binding. The

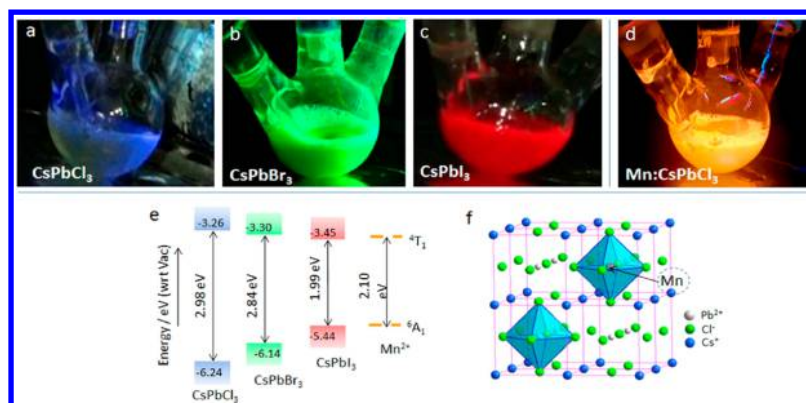


Figure 4. (a–d) Photographs of CsPbCl₃, CsPbBr₃, CsPbI₃, and Mn:CsPbCl₃ nanocrystals in a reaction flask illuminated with UV light. (e) VB and CB positions of CsPbX₃ and Mn d-states. (f) Atomic model showing a typical Mn:CsPbCl₃ crystal where Mn is placed in the position of Pb. Reprinted with permission from ref 62. Copyright 2017 American Chemical Society.

most straightforward method is to adapt synthetic pathways developed for classical binary CdSe, PbS, and related CSQDs to alternative metal cations. Initially, this strategy was successfully used in the case of zinc chalcogenide nanocrystals, in particular, ZnSe QDs⁵⁶ synthesized by a variety of heat-up and hot-injection methods. However, this approach has met limited success, as the emission of zinc chalcogenide NCs is restricted to the UV and blue spectral range, and the reported PL QYs are significantly lower than with Cd-chalcogenides.

In the case of metal halide perovskites, a comparable approach can also be applied: instead of lead halide precursors, Sn²⁺ salts can be used to produce all-inorganic CsSnX₃ NCs by classical hot-injection methods resulting in perovskites with 3D dimensionality (i.e., corner-sharing SnX₆ octahedra).^{57,58} However, in contrast to their Pb-based counterparts, the resulting CsSnX₃ HPNCs show low PL QY (<0.14%) because of the presence of shallow intrinsic defect sites and are very unstable due to the inherent oxidation sensitivity of Sn²⁺. Improved QY and stability can be obtained by synthesizing CsSnBr₃ nanocrystals in a nanocage morphology and treating them with perfluorooctanoic acid acting as stabilizer for Sn²⁺.⁵⁷

Another example of isovalent replacement is copper(II)-based perovskite NCs, which could be synthesized using the so-called ligand-assisted reprecipitation (LARP) technique at room temperature.⁵⁹ In this work a Cs₂CuBr₄ structure is claimed; however, the authors also observe the presence of Cu⁺ in the material, and no information about the resulting dimensionality of the perovskite structure is available.

Partial Precursor Replacement. Another strategy to render CSQDs more environmentally friendly is to reduce the fraction of toxic heavy metals. The use of Cd together with nontoxic metal precursors during the synthesis allows us to incorporate them in the final CSQDs to obtain alloyed Zn_xCd_{1-x}S, Zn_xCd_{1-x}Se, or similar compounds.⁶⁰ In addition to the partial Cd replacement, nanoscale alloying can result in a combination of advantages like enhanced stability and highly tunable PL from blue to the near-infrared with improved efficiency, which is rarely achievable with the parent binary systems and can open new perspectives for applications.

By using an analogous approach with perovskite nanocrystals and applying the hot-injection synthesis, it is possible to prepare alloyed HPNCs, typically having the formula CsPb_{1-y}M_yX₃. The most studied examples are manganese-substituted NCs of type CsPbMnX₃ (where X is usually

chloride, cf. Figure 4) for several reasons: (i) Mn²⁺ has been widely used as a dopant in CSQDs for forming dilute magnetic semiconductors;⁶¹ (ii) it opens the way toward exciting optical properties related to energy transfer to the d-state of Mn²⁺ favorably located within the HPNC gap; (iii) bond energies of Pb–X and Mn–X are comparable, which is a prerequisite for an efficient exchange. The ease of the replacement coupled to the impressive optical benefits gained by partial Mn substitution or doping made this field one of the most dynamically developing among HPNCs with several dozens of papers already published.⁶² Usually the doping ratio does not exceed 3%, but in some cases it was possible to reach a much higher Pb replacement with Mn, up to 54% with inorganic CsPb_xMn_{1-x}Cl₃⁶³ and 90% with MAPb_{1-x}Mn_xBr_{3-(2x+1)Cl_{2x+1} NCs (a rare example of B-site exchanged organic–inorganic HPNCs),⁶⁴ while keeping the HPNCs highly emissive.}

Other examples of successful B-site partial substitution in CsPbX₃ NCs include Ni²⁺⁶⁵ and Sr²⁺.⁶⁶ These approaches not only allow reducing the lead contents in HPNCs but can also result in high PL QYs^{65,67} and improved stability,^{66,68} enabling first applications of doped HPNCs in light-emitting devices.^{66,69}

Remarkable results were achieved by incorporating Sn²⁺ precursors in the hot-injection synthesis of alloyed CsPbSnX₃ HPNCs. For example, by alloying tin and lead in iodide perovskite, CsPb_{1-x}Sn_xI₃ with high Sn contents can be obtained with a phase stability for months in solution, which is superior to both CsPbI₃ and CsSnI₃ and enabled the design of solar cells using lead-deficient HPNCs.⁷⁰ By using CsPb_{1-x}Sn_xBr₃ NCs, efficient and stable light-emitting devices were fabricated.⁷¹

Postsynthetic Ion Exchange. An interesting way to synthesize less toxic CSQDs is ion exchange on presynthesized NCs.^{72,73} This approach is especially well suited for metal chalcogenides due to relatively high ionicity of their structures (especially compared to III–V compounds). Metal cations have a higher mobility in the crystalline lattice than (larger) anions and easily undergo exchange, enabling for example sequential conversions like CdSe → Cu₂Se → ZnSe under conservation of the size and shape of the NCs.⁷⁴ Even more sophisticated exchanges are possible by this method, such as partial copper replacement by indium to obtain ternary NCs (Cu₂S → CuInS₂) followed by partial Cu and In replacement by Zn (CuInS₂ → (CuInZn)S₂).⁷⁵ Moreover, this

powerful technique can even be applied in a similar fashion for heterostructures, such as for example efficient transformation from toxic CdSe/CdS to cadmium-free CuInSe₂/CuInS₂ heteronanorods.⁷⁶

In the case of HPNCs the bonds are more ionic compared to CSQDs, thus in principle rendering similar ion exchange even easier. Owing to their single charge and their high vacancy concentration, anion exchange has become one of the signature features of HPNCs.^{22,23} Even though this efficient process is versatile and allows tuning optical and electronic properties of HPNCs in a wide range, it does not decrease their potential toxicity. Meanwhile, it is also possible to realize cation exchange of the perovskite B-site, namely, replace lead with alternative elements. In addition to decreasing the overall materials toxicity by reducing the lead concentration, this strategy can improve the structural and thermal stability of HPNCs. As an example, partial Pb replacement can stabilize crystalline phases by limiting the octahedral rotation tilt.⁶⁸ However, in contrast to CSQDs, the postsynthetic cation exchange process for HPNCs is still in its infancy with a limited success as it is much more challenging to exchange divalent lead once it is already strongly coordinated within the center of the halogen octahedral cage, considerably limiting its mobility. In addition, there are very few divalent cation vacancies and very limited space for interstitials in the perovskite materials, all this leading to high activation energies calculated for cationic migration (2.31 eV for Pb²⁺ compared to 0.58 eV for I⁻ in CH₃NH₃PbI₃).⁷⁷ Finally, the size of the B-cations should be compatible with the above-mentioned Goldschmidt tolerance and octahedral factors. As a result, very few examples of such B-site cation exchange were reported to date. To give an example, Donega et al. studied lead replacement in CsPbBr₃ NCs with various metal cations.⁷⁸ By using high-resolution spectroscopy and fluorescence methods they demonstrated incorporation of Cd, Zn, and Sn cations into the perovskite lattice, albeit replacing lead only partially with the final M/Pb ratios of 0.16, 0.05, and 0.1 (Figure 5). It was also possible to incorporate Mn²⁺ by

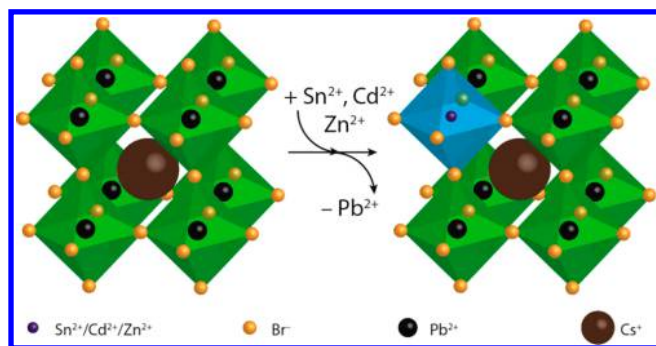


Figure 5. Schematic overview of partial cation exchange in CsPbBr₃ nanocrystals. Pb²⁺ cations are partially replaced by other divalent cations (Sn²⁺, Cd²⁺, and Zn²⁺) by postsynthetic cation exchange reactions. Reprinted with permission from ref 78. Copyright 2017 American Chemical Society.

postsynthetic cation exchange into the CsPbCl₃ matrix using MnCl₂.⁷⁹ Finally, another interesting way of Pb substitution in presynthesized HPNCs is combined cation–anion exchange, which allows replacing up to 2% of Pb simultaneously with Br in CsPbBr₃ to convert it to CsPbMnCl₃.⁸⁰

These examples demonstrate the feasibility of B-site cation exchange, inspired by procedures developed for CSQDs, but at the same time also expose the difficulties and limitations of its application in the case of HPNCs.

4.2. Heterovalent Atom Replacement. One of the most successful examples of less toxic CSQD alternatives to classic CdSe is indium phosphide, InP. The major interest of this III–V material originates from its tunable emission in the visible and NIR range similarly to that of CdSe NCs. Initial syntheses were hampered by long reaction times of several days related to the use of coordinating solvents (trioctylphosphine oxide).⁸¹ The introduction of meanwhile ubiquitously applied 1-octadecene as noncoordinating solvent enabled faster reactions and yielded narrower size distributions,⁸² even though up until now no efficient way for decreasing the emission line width to similar values as with Cd-chalcogenide nanocrystals has been found, the best values being 36–39 nm (fwhm) for an emission in the range of 533–625 nm (Figure 6).⁸³ Similarly, as in the case of Cd-chalcogenides the growth of inorganic shells on InP or In(Zn)P core QDs led to a significant improvement of the PL QY, in the best cases exceeding 80%.^{84,85}

In the example of CdSe substitution by InP, both the metal cation and the chalcogenide anion are replaced by heteroelements. Keeping the chalcogenide anion while substituting Cd with heterovalent metal ions in CSQDs imposes the design of multinary compounds due to the requirement of charge balance. One illustrative example is the replacement of the divalent Cd²⁺ ion by a combination of a monovalent Cu⁺ and a trivalent In³⁺ ion in CuInS₂ or CuInSe₂ (vide infra). To the contrary, perovskite materials offer the unique possibility to form so-called “vacancy ordered” structures accommodating heterovalent elements directly in the perovskite lattice. To compensate the different charge of the incorporated elements, void BX₃ octahedra are intercalated in an organized manner with those filled by these new elements, thus doubling or tripling the unit cell (Figure 7). This structure allows accommodating a series of tri- and even tetravalent elements while maintaining the perovskite lattice (albeit usually with decreased perovskite dimensionality). Moreover, such an arrangement allows for producing nanomaterials with very interesting optical properties and high stability.

The most studied examples of such lead-free vacancy ordered perovskites are bismuth(III)-based ones for several reasons: bismuth is a nontoxic element; moreover, it is isoelectronic (6s²6p⁰) to lead, which may lead to similarly high defect tolerance. Due to the ordered defect structure, Bi-based perovskite NCs have lower perovskite dimensionality: generally 2D for bromides (Cs₃Bi₂Br₉ and MA₃Bi₂Br₉), 1D for chlorides (MA₃Bi₂Cl₉), down to 0D for iodides (Cs₃Bi₂I₉ and MA₃Bi₂I₉).⁸⁷ Bi-based HPNCs have typically large band gaps, making them particularly interesting emitters in the UV and blue regions, which are almost not covered by smaller band gap lead halide perovskite NCs. For example, recently, blue-emitting MA₃Bi₂Br₉ NCs with high PL QY of 54% were obtained by passivating the surface.⁸⁸ Also, it was shown that the Cs₃Bi₂Br₉ NCs can be stable in the ambient conditions for over 30 days.⁸⁹

Replacing three Pb²⁺ ions in the perovskite structure by the two Sb³⁺ results in nanocrystals with a band gap in the visible range. The radius of antimony fits the geometrical Goldschmidt tolerance factor, allowing us to yield stable 2D structures with blue emission for Cs₃Sb₂Br₉⁹⁰ and yellow to

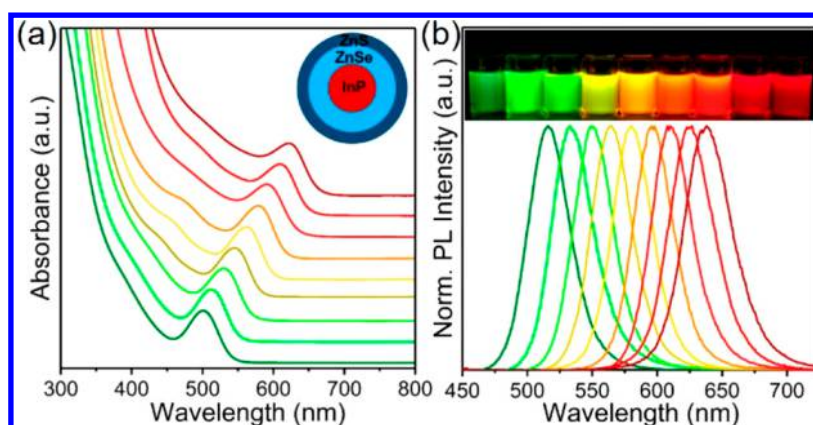


Figure 6. UV-vis absorption (a) and PL (b) spectra of a size series of InP/ZnSe/ZnS core/shell QDs synthesized using a seed-mediated approach with core sizes in the range of 1.9–4.5 nm (size distributions: 4–9%, emission line widths: 36–39 nm fwhm). Reprinted with permission from ref 83. Copyright 2018 American Chemical Society.

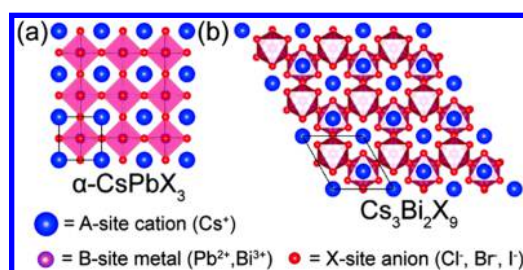


Figure 7. Illustration of a vacancy ordered perovskite structure. Reprinted with permission from ref 86. Copyright 2018 Royal Society of Chemistry.

red emission for $\text{Cs}(\text{Rb})_3\text{Sb}_2\text{I}_9$ HPNCs. However, lead replacement comes at the cost of increased tendency of such materials for the formation of defects situated within the band gap. Finally, a logical candidate for the heterovalent lead replacement is Sn^{4+} : despite its chemical similarity to the Pb^{2+} , it is much more stable compared to its divalent analogue. Cs_2SnI_6 HPNCs of different shapes could be prepared by classical hot-injection synthesis using tin(IV) precursors with a possibility of forming films with high hole mobility.⁹¹ Taking advantage of the good solubility of SnI_4 in octadecene solvent, ligand-free and stable Cs_2SnI_6 HPNCs could be synthesized.⁹²

Heterovalent ion impurity incorporation in CSQDs can be a powerful tool to modulate the conductivity and induce n- or p-electronic doping, opening the ways for their use in heterojunction solar cells.^{93,94} At the same time, successful examples of such doping are extremely rare because obtaining heterovalently doped NCs while maintaining the luminescence properties is not a trivial task owing to the quenching on the trap states induced by the uncompensated charges.⁹⁵ Due to the great compositional flexibility of the HPNCs, heterovalent ion introduction into the lead-based crystalline lattice was recently achieved yielding compounds not only stable but also with improved PL efficiency. For example, lanthanide cations were successfully incorporated during the hot-injection synthesis into CsPbX_3 NCs with a ratio up to 9% leading to a significantly improved QY and tunable emission.^{69,96,97} Similar Eu^{3+} and Tb^{3+} incorporation was achieved using one-pot ultrasonic synthesis.⁹⁸ Doping by minute amounts of trivalent Al and Bi can also result in emissive alloyed CsPbBr_3 NCs with very intriguing optical properties.^{99,100} Tetravalent tin incorporation in alloyed $\text{CsPb}_{1-x}\text{Sn}_x\text{Br}_3$ NCs was recently

demonstrated: by replacing 33% of lead with a stable Sn^{4+} cation, it was possible to reach PL QYs up to 83% and to fabricate efficient light-emitting devices with high stability.¹⁰¹

As in the case of CSQDs, the great potential of electronic doping of HPNCs for tuning the optical, magnetic, and electronic properties remains still relatively underexplored.

4.3. Heteroelement Replacement. In the field of CSQDs a powerful strategy to enlarge the variety of materials of interest and to access toxic heavy metal-free semiconductors with bulk band gap energies < 2 eV consists of switching from binary to ternary or more generally multinary NCs. A classic example is the well-studied case of metal chalcogenides when going from II–VI to I–III–VI₂ semiconductors with the benchmark examples of CdS (CdSe) and CuInS_2 (CuInSe_2) NCs. Divalent Cd cations are replaced in the synthetic procedure by a mixture of monovalent copper and trivalent indium, occupying the metal sites in the crystalline lattice. I–III–VI₂ semiconductors typically crystallize in the tetragonal chalcopyrite or the cubic zinc blende structure. As an important characteristic, such ternary CSQDs can tolerate large off stoichiometries, widening the range of achievable optoelectronic properties compared to binary nanostructures.¹⁰² At the same time this feature is, however, at the origin of a complex, size, and composition-dependent electronic structure characterized by a large variety of defect states.¹⁰³

By developing a very simple synthetic scheme where 1-dodecanethiol (DDT) acts as the sulfur source, surface ligand, and (co)solvent, CuInS_2 (CIS) NCs of narrow size distribution and high PL QY of 60% after ZnS shell growth could be obtained.^{104,105} Initial studies of the photophysical properties of these materials highlighted the importance of localized intra-band gap-states in the optical transitions.¹⁰⁶ The current understanding of the emission properties of CIS nanocrystals, based on single-particle studies, suggests a free-to-bound mechanism in which the photogenerated electron is delocalized in the conduction band, while the hole is localized on Cu-related intra-band-gap defect states.¹⁰⁷ This model is in accordance with experimental results showing large Stokes shifts and emission line widths (> 150 meV) in combination with comparably long PL decay times of several hundreds of nanoseconds.^{108,109} A recent combined study by NMR spectroscopy and synchrotron X-ray diffraction allowed identifying the growth mechanism via a 2D lamellar phase

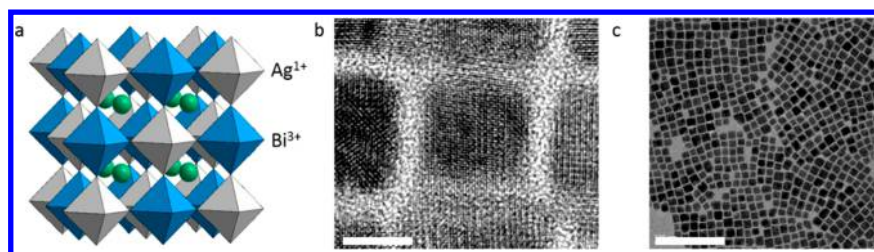


Figure 8. (a) Cartoon of the extended unit cell of a $\text{Cs}_2\text{AgBiX}_6$ lead-free double perovskite (gray and blue depict the Ag(I) and Bi(III) octahedra, respectively; Cs atoms are shown in green). (b) High-resolution TEM image of $\text{Cs}_2\text{AgBiBr}_6$ NCs showing atomic lattice fringes, and the faceted cubic shape of the crystals (scale bar: 8 nm). (c) Low-resolution TEM image of the same sample (scale bar: 100 nm). Reprinted with permission from ref 121. Copyright 2018 American Chemical Society.

and unraveling an intriguing surface composition of CIS NCs prepared with the DDT method.¹¹⁰ In particular, the formation of a dense ligand double layer consisting of dodecanethiolate and *in situ* formed didodecylsulfide has been identified. Due to the high chemical stability and interesting electronic and optical properties of these nanomaterials, they have been successfully used in a variety of applications: for biolabeling,^{104,105} hybrid¹¹¹ and sensitized^{112–114} solar cells, photodetectors,¹¹⁵ and more recently photocatalytic hydrogen production.¹¹⁶ At present, a multitude of potential applications of CuInS_2 NCs exist,¹¹⁷ and first examples of their commercialization¹¹⁸ appear, making this type of nanocrystal one of the frontrunners among safer-by-design CSQDs.

The present approach can be pushed further by going from ternary to quaternary CSQDs: in order to replace (scarce) In in I–III–VI₂ structures, I₂–II–IV–VI₄ analogues can be prepared, as represented by $\text{Cu}_2\text{ZnSnS}_4$ and related compounds usually crystallizing in the tetragonal kesterite phase. Because of the increased elemental variety and the flexibility of the structure, an even larger spectrum of off-stoichiometric compounds is possible to achieve using this structure. On one hand, this allows fine-tuning of the optoelectronic properties of the obtained NCs. However, the same chemical diversity can present a hurdle as various secondary binary and ternary phases can be thermodynamically stable, introducing a heterogeneity into the material, which is often detrimental for the sought applications.¹¹⁹ The synthesis of kesterites in the form of colloidal nanocrystals can give a better control over the structural and chemical homogeneity of the material.¹²⁰

In the case of HPNCs a similar strategy can be considered: divalent lead can be replaced by two heterovalent elements, such as for example monovalent Ag and trivalent Bi, giving rise to elpasolite (or “double perovskite”) structures. It is relatively challenging to fabricate thin crystalline films of the elpasolites because of the poor solubility of the precursors and the relative instability of the final materials. Similar to the previously mentioned kesterites, the approach relying on colloidal NCs could be an interesting alternative here. Recently, a series of such HPNCs were synthesized ($\text{Cs}_2\text{AgBiCl}_6$, $\text{Cs}_2\text{AgBiBr}_6$, $\text{Cs}_2\text{AgBiI}_6$, as well as the mixed halides), demonstrating indirect band gaps in the range of 2–2.9 eV and consequently generally rather low photoluminescence (PLQY < 7%) strongly dependent on the surface passivation and the presence of defects (Figure 8).^{121–123}

The nature of the photoluminescence of the $\text{Cs}_2\text{AgBiX}_6$ elpasolites is still under debate, with some reports claiming

that it originates from quantum confinement,^{122,124} while others identify it as a localized Bi 6s–6p transition of a nonconfined exciton.¹²¹ The PL QY can be significantly improved (up to 16%) by using the previously described approach of Mn doping, taking advantage of the Mn^{2+} emission sensitization by the elpasolite core.¹²⁵ Careful ligand engineering can result in NCs with a stability overpassing that of Pb-based nanocrystals.¹²⁴ Figure 9 summarizes the different approaches outlined of heterovalent and heteroelement replacement of lead in HPNCs.

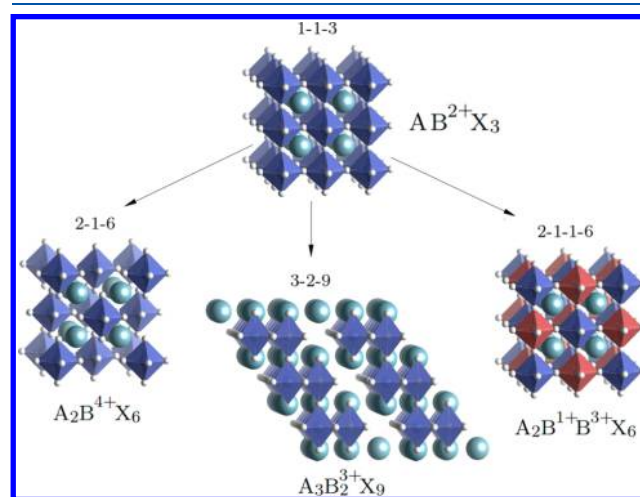


Figure 9. Stoichiometries observed in the case of heterovalent substitution of lead in HPNCs using tri- or tetravalent metal ions on the B-site and of heteroelement replacement using a combination of mono- and trivalent metal ions, leading to double perovskites. Reproduced with permission from ref 126. Copyright 2016 American Chemical Society.

5. CONCLUSIONS AND PERSPECTIVES

As demonstrated in this article, the emerging field of HPNCs is developing extremely fast. In a very short time a huge amount of unique photophysical properties has been discovered along with a broad structural diversity. The broad knowledge accumulated over more than three decades in the field of CSQDs as well as more recent innovations in the field of metal halide perovskite based photovoltaics enabled this rapid evolution. In the case of CSQDs viable alternatives to Cd- and Pb-based NCs are becoming established, with the most promising to date in terms of PL properties being InP-based and ternary QDs, such as CuInS_2 , AgInS_2 NCs, and the like. The replacement of lead in HPNCs, on the other hand, is a difficult task due to their distinct

electronic structure related to the Pb^{2+} ion, resulting in a high defect tolerance and absence of deep midgap trap states. For the rational design of novel lead-free perovskites, computational methods are of great help. First-principles calculations can significantly narrow down the choice of potentially interesting materials by predicting the stability and optoelectronic properties. Therefore, computational tools can tremendously accelerate the discovery of new materials by rapid screening and save a lot of synthetic research efforts.¹²⁷ Very recently, a powerful screening approach has been proposed based not only on structural and electronic simulations but also on Internet data mining and inferential statistics.¹²⁸ Meanwhile, computational methods generally have the notorious drawback of failing to discover metastable phases and can thus ignore potentially interesting compositions. With this in mind, for the design and prediction of new HPNC compositions a rational experimental material screening should not be underestimated. Recently, two promising approaches allowing the rapid synthesis and test of a large variety of novel perovskite NCs have been reported: a high-throughput robot-assisted method¹²⁹ and continuous synthesis using a droplet-based microfluidic platform.¹³⁰

Shell Growth and Surface Treatment Strategies. A rich history of inorganic shell passivation of CSQDs allows now understanding of the underlying mechanisms of the shell growth, as well as its effects on the properties of the nanocrystals.¹⁰ A semiconductor shell can greatly enhance the stability and optical properties of CSQDs by protecting their surface and confining photogenerated excitons in the core, respectively. A variety of synthetic strategies has been developed (e.g., SILAR - successive ionic layer adsorption and reaction and cation exchange approaches) to grow shells of precisely controlled thickness and composition on many types of CSQDs, making the shell passivation almost a routine step for the fabrication of robust QDs.

In the case of HPNCs the situation is different: even though stability issues are also limiting the applications of these materials, the shell growth is far from being well understood and widely used in this field. The same applies to surface ligand chemistry: generally the same types of ligands (e.g., oleic acid, oleylamine) are used as in the case of established CSQDs, and only a few examples of novel types of ligands yielding enhanced stability exist. One of the reasons is that surface passivation with a shell is less critical for the optical properties of lead-based HPNCs compared to CSQDs, as the former already exhibit very high PLQYs in their pristine state. However, in the case of safer-by-design (Pb-free) HPNCs the optical properties are often much more strongly dependent on defects and impurities. In some cases, their stability is intrinsically lower than that of lead-containing ones (for example for Sn^{2+} -based HPNCs); however, switching to 2D perovskites can enable the design of Pb-free materials of enhanced stability suitable for use in applications.¹³¹

In the literature, examples of successful shell growth on HPNCs are still very scarce.⁵⁰ The shells typically used for CSQDs, such as wide band gap ZnS or similar materials, are often not applicable for the HPNCs because of precursors' incompatibility and/or too high crystallographic lattice mismatch. To date, the best working alternative strategies to improve the stability comprise embedding HPNCs into oxide (SiO_2 , TiO_2 , Al_2O_3) or polymeric matrices, which however often strongly limit or impede their further dispersibility in solvents and thus their practical use. Another original strategy

takes advantage of the similar chemical and crystalline properties of different perovskites with discontinuous structural dimensionality and band gaps to construct core/shell systems. The use of a 2D layered perovskite shell on the surface of 3D MAPbBr_3 cores is an appealing example developed by Mathews and co-workers, which allowed greatly improving the stability and PL QY.¹³² Another original example of successful shell formation was achieved by combining a crystalline perovskite core with an amorphous perovskite shell of the same composition.¹³³

Probably the most straightforward way to grow a wider band gap shell compatible with the optically active core would be to combine perovskites with different halides; however, this approach is ineffective: due to the high halide ionic mobility in HPNCs, rather alloyed mixed halide NCs would form instead of heteronanostructures. Conversely, this strategy can become fruitful for safer-by-design HPNCs: for a series of NCs halide exchange is much less energetically favorable, opening the way for shell engineering with the same family of perovskites. This approach has been successfully explored for $\text{Cs}_3\text{Bi}_2\text{Br}_9/\text{Cs}_3\text{Bi}_2\text{Cl}_9$ perovskite core/shell structures,⁸⁸ however, it should be applicable for a much broader range of Pb-free HPNCs. Improved environmental stability is obviously most crucial for Sn^{2+} HPNCs, which are extremely sensitive to oxidation.

For a range of applications comprising photocatalysis some safer-by-design HPNCs can turn out very useful because of the high absorption coefficient coupled with energy levels favorably situated for water splitting or CO_2 reduction, either as photosensitizers or directly as photocatalysts (or cocatalysts). However, water-splitting environments imply the use of NCs stable in aqueous solution, which is typically unachievable using conventional Pb-based HPNCs because of their common incompatibility with water resulting from their high ionicity. Recently, several surface treatment strategies have been proposed to circumvent this problem and render lead-based HPNCs water-compatible while maintaining their luminescence. For example, Xu et al. developed a direct aqueous synthesis of HPNCs based on a complexed form of lead halide and acidic pH, leading to water-stable MAPbBr_3 colloidal solutions.¹³⁴ Another strategy capable of drastically improving the stability of perovskite nanoparticles in water consists of introducing a siloxane coating on their surface, leading to highly luminescent CsPbX_3 nanopowders.¹³⁵ Even though no examples of water-compatible lead-free nanocrystals have been reported so far, the strategies described above can be sufficiently versatile to be adapted for this type of materials to make them more attractive for applications involving aqueous media (such as, for example, photocatalysis) or requiring high humidity resistance.

Doping. Doping is an established powerful tool for improving or modifying the PL properties of CSQDs.¹³⁶ In the case of HPNCs in general and lead-free ones in particular, the arsenal of synthetic tools for PL enhancement is more limited due to the difficulties exposed in the previous paragraph. Moreover, the PL of some nanocrystals, which are very compositionally promising and structurally intriguing, such as for example recently synthesized elpasolite HPNCs, is weak and critically needs improving. In this case using doping of an appropriate nature and concentration can open the way toward completely lead-free perovskite NCs with attractive optical properties. The first examples of such impurity engineering using Mn^{2+} for double perovskites start to appear,

allowing us to improve the PL QY 10-fold¹²⁵ and could be extended on other compositions. Another example of extremely efficient doping into lead-free HPNCs is hetero-valent Bi³⁺ dopant incorporation into tin-based perovskite Cs₂SnCl₆ rendering initially nonluminescent NCs highly emissive with QY close to 80%¹³⁷ and proving that the choice of the dopant ions is not limited to the isovalent elements and thus could be applied to a variety of lead-free HPNCs. Finally, an original way of getting the white-light emission from the HPNCs was developed by introducing two dopant ions with distinct levels (Bi³⁺ and Mn²⁺) together into CsPbCl₃.¹³⁸ Such codoping approaches can be easily extended to lead-free perovskite NCs for the use as white light emitters.

Near-Infrared Materials. Finally, another field of high interest, which requires substantial development in terms of both toxic heavy metal free CSQDs and HPNCs is the field of near-infrared absorbers/emitters. In the case of CSQDs, this domain is dominated by lead and mercury chalcogenide nanocrystals,⁴² while narrow band gap safer-by-design materials (e.g., copper-, silver-, or iron-based binary or multinary nanocrystals) exhibit so far much lower quality of the optical properties. The band gaps currently available with HPNCs do not allow achieving materials having an absorption onset and emission peak beyond 1 μm, and the lowest band gap materials theoretically predicted remain to be synthesized experimentally.¹³⁹ This spectral region is of particular interest for many applications including photodetectors, absorbers for multiple junction solar cells, in vivo imaging, gas sensing, and so on.

Concluding, the cross-fertilizing fields of CSQDs and HPNCs provide a very prolific playground for research, in particular in the development of novel materials with tailor-made optical and electronic properties for numerous applications ranging from energy conversion (e.g., photovoltaics and photocatalysis) over photodetection and light emission (white light generation, displays, lasing, etc.) to biological imaging, detection, and theranostics. Because the huge research interest in these fields is currently draining, it can be expected that many of the above-listed challenges can be leveraged in the near future.

AUTHOR INFORMATION

Corresponding Authors

*E-mail: dmitry.aldakov@cea.fr.

*E-mail: peter.reiss@cea.fr.

ORCID

Dmitry Aldakov: 0000-0002-4581-2462

Peter Reiss: 0000-0002-9563-238X

Author Contributions

The manuscript was written through contributions of all authors. All authors have given approval to the final version of the manuscript.

Notes

The authors declare no competing financial interest.

Biographies



Dmitry Aldakov is currently a CNRS researcher at the SyMMES laboratory at CEA-Grenoble (France). Following his graduation from Mendeleev University (Moscow, Russia) in 1999 and earning his Ph.D. in Chemistry from Bowling Green State University (United States) in 2004, he performed postdoctoral stays at the CEA-Grenoble and Ecole Polytechnique (France) before joining the CNRS at 2011. His current research interests include third-generation solar cells, photocatalytic hydrogen production, perovskite materials, quantum dots, and interface characterization.



Peter Reiss is a researcher at CEA Grenoble, SyMMES Laboratory, and head of the team Synthesis, Structure and Properties of Functional Materials (STEP). He graduated in 1997 from the University of Karlsruhe (Germany) and earned his Ph.D. in Inorganic Chemistry under the supervision of Prof. Dieter Fenske (2000). His research activities focus on colloidal semiconductor nanocrystals and nanowires, in particular their synthesis, surface functionalization, and assembly of these nanoscale building blocks into structurally controlled functional materials. The studied applications range from fluorescent markers for biological labeling and detection over the development of efficient emitters for LEDs and displays to new strategies for nanocrystal-based energy conversion (photovoltaics, thermoelectrics) and storage.

ACKNOWLEDGMENTS

The authors thank the French National Research Agency ANR (grants SuperSansPlomb: ANR-15-CE05-0023-01, PER-SIL: ANR-16-CE05-0019-02, NEUTRINOS: ANR-16-CE09-0015-03, FLUO: ANR-18-CE09-0039-01) as well as LABEX ARCANE (ANR-11-LABX-0003-01) for financial support.

REFERENCES

- (1) Efros, A. L.; Efros, A. L. Interband Absorption of Light in a Semiconductor Sphere. *Sov. Phys. Semicond.* **1982**, *16*, 772–775.
- (2) Henglein, A. Photo-degradation and Fluorescence of Colloidal-Cadmium Sulfide in Aqueous-Solution. *Ber. Bunsen-Ges.-Phys. Chem. Chem. Phys.* **1982**, *86*, 301–305.
- (3) Rossetti, R.; Brus, L. Electron-Hole Recombination Emission as a Probe of Surface Chemistry in Aqueous Cadmium Sulfide Colloids. *J. Phys. Chem.* **1982**, *86*, 4470–4472.
- (4) Brus, L. E. Electron–Electron and Electron–Hole Interactions in Small Semiconductor Crystallites: The Size Dependence of the Lowest Excited Electronic State. *J. Chem. Phys.* **1984**, *80*, 4403–4409.
- (5) Ekimov, A. I.; Onushchenko, A. A. Quantum Size Effect in Three-Dimensional Microscopic Semiconductor Crystals. *JETP Lett.* **1981**, *34*, 345–349.
- (6) Ekimov, A. I.; Onushchenko, A. A. Quantum Size Effect in the Optical-Spectra of Semiconductor Microcrystals. *Sov. Phys. Semicond.* **1982**, *16*, 775–778.
- (7) Itoh, T.; Kirihara, T. Excitons in CuCl Microcrystals Embedded in NaCl. *J. Lumin.* **1984**, *31–32*, 120–122.
- (8) Murray, C. B.; Norris, D. J.; Bawendi, M. G. Synthesis and Characterization of Nearly Monodisperse Cde (E = S, Se, Te) Semiconductor Nanocrystallites. *J. Am. Chem. Soc.* **1993**, *115*, 8706–8715.
- (9) Hines, M. A.; Guyot-Sionnest, P. Synthesis and Characterization of Strongly Luminescing ZnS-Capped CdSe Nanocrystals. *J. Phys. Chem.* **1996**, *100*, 468–471.
- (10) Reiss, P.; Protière, M.; Li, L. Core/Shell Semiconductor Nanocrystals. *Small* **2009**, *5*, 154–168.
- (11) Gretyak, A. B.; Allen, P. M.; Liu, W.; Zhao, J.; Young, E. R.; Popović, Z.; Walker, B. J.; Nocera, D. G.; Bawendi, M. G. Alternating Layer Addition Approach to CdSe/CdS Core/Shell Quantum Dots with Near-Unity Quantum Yield and High on-Time Fractions. *Chem. Sci.* **2012**, *3*, 2028–2034.
- (12) Pietryga, J. M.; Park, Y.-S.; Lim, J.; Fidler, A. F.; Bae, W. K.; Brovelli, S.; Klimov, V. I. Spectroscopic and Device Aspects of Nanocrystal Quantum Dots. *Chem. Rev.* **2016**, *116*, 10513–10622.
- (13) Wegner, K. D.; Hildebrandt, N. Quantum Dots: Bright and Versatile in Vitro and in Vivo Fluorescence Imaging Biosensors. *Chem. Soc. Rev.* **2015**, *44*, 4792–4834.
- (14) Reiss, P.; Carrière, M.; Lincheneau, C.; Vaure, L.; Tamang, S. Synthesis of Semiconductor Nanocrystals, Focusing on Nontoxic and Earth-Abundant Materials. *Chem. Rev.* **2016**, *116*, 10731–10819.
- (15) Xu, G.; Zeng, S.; Zhang, B.; Swihart, M. T.; Yong, K.-T.; Prasad, P. N. New Generation Cadmium-Free Quantum Dots for Biophotonics and Nanomedicine. *Chem. Rev.* **2016**, *116*, 12234–12327.
- (16) Schmidt, L. C.; Pertegás, A.; González-Carrero, S.; Malinkiewicz, O.; Agouram, S.; Mínguez Espallargas, G.; Bolink, H. J.; Galian, R. E.; Pérez-Prieto, J. Nontemplate Synthesis of CH₃NH₃PbBr₃ Perovskite Nanoparticles. *J. Am. Chem. Soc.* **2014**, *136*, 850–853.
- (17) Gonzalez-Carrero, S.; Galian, R. E.; Perez-Prieto, J. Maximizing the Emissive Properties of CH₃NH₃PbBr₃ Perovskite Nanoparticles. *J. Mater. Chem. A* **2015**, *3*, 9187–9193.
- (18) Zhang, F.; Zhong, H.; Chen, C.; Wu, X.-G.; Hu, X.; Huang, H.; Han, J.; Zou, B.; Dong, Y. Brightly Luminescent and Color-Tunable Colloidal CH₃NH₃PbX₃ (X = Br, I, Cl) Quantum Dots: Potential Alternatives for Display Technology. *ACS Nano* **2015**, *9*, 4533–4542.
- (19) Lee, M. M.; Teuscher, J.; Miyasaka, T.; Murakami, T. N.; Snaith, H. J. Efficient Hybrid Solar Cells Based on Meso-Structured Organometal Halide Perovskites. *Science* **2012**, *338*, 643–647.
- (20) Kim, H. S.; Lee, C. R.; Im, J. H.; Lee, K. B.; Moehl, T.; Marchioro, A.; Moon, S. J.; Humphry-Baker, R.; Yum, J. H.; Moser, J. E.; et al. Lead Iodide Perovskite Sensitized All-Solid-State Submicron Thin Film Mesoscopic Solar Cell with Efficiency Exceeding 9%. *Sci. Rep.* **2012**, *2*, 591.
- (21) Protesescu, L.; Yakunin, S.; Bodnarchuk, M. I.; Krieg, F.; Caputo, R.; Hendon, C. H.; Yang, R. X.; Walsh, A.; Kovalenko, M. V. Nanocrystals of Cesium Lead Halide Perovskites (CsPbX₃, X = Cl, Br, and I): Novel Optoelectronic Materials Showing Bright Emission with Wide Color Gamut. *Nano Lett.* **2015**, *15*, 3692–3696.
- (22) Nedelcu, G.; Protesescu, L.; Yakunin, S.; Bodnarchuk, M. I.; Grotevent, M. J.; Kovalenko, M. V. Fast Anion-Exchange in Highly Luminescent Nanocrystals of Cesium Lead Halide Perovskites (CsPbX₃, X = Cl, Br, I). *Nano Lett.* **2015**, *15*, 5635–5640.
- (23) Akkerman, Q. A.; D’Innocenzo, V.; Accornero, S.; Scarpellini, A.; Petrozza, A.; Prato, M.; Manna, L. Tuning the Optical Properties of Cesium Lead Halide Perovskite Nanocrystals by Anion Exchange Reactions. *J. Am. Chem. Soc.* **2015**, *137*, 10276–10281.
- (24) Li, J.; Bouchard, M.; Reiss, P.; Aldakov, D.; Pouget, S.; Demadrille, R.; Aumaitre, C.; Frick, B.; Djurado, D.; Rossi, M.; et al. Activation Energy of Organic Cation Rotation in CH₃NH₃PbI₃ and CD₃NH₃PbI₃: Quasi-Elastic Neutron Scattering Measurements and First-Principles Analysis Including Nuclear Quantum Effects. *J. Phys. Chem. Lett.* **2018**, *9*, 3969–3977.
- (25) Juarez-Perez, E. J.; Sanchez, R. S.; Badia, L.; Garcia-Belmonte, G.; Kang, Y. S.; Mora-Sero, I.; Bisquert, J. Photoinduced Giant Dielectric Constant in Lead Halide Perovskite Solar Cells. *J. Phys. Chem. Lett.* **2014**, *5*, 2390–2394.
- (26) Miyata, A.; Mitioglu, A.; Plochocka, P.; Portugall, O.; Wang, J. T.-W.; Stranks, S. D.; Snaith, H. J.; Nicholas, R. J. Direct Measurement of the Exciton Binding Energy and Effective Masses for Charge Carriers in Organic–Inorganic Tri-halide Perovskites. *Nat. Phys.* **2015**, *11*, 582–587.
- (27) Droseros, N.; Longo, G.; Brauer, J. C.; Sessolo, M.; Bolink, H. J.; Banerji, N. Origin of the Enhanced Photoluminescence Quantum Yield in MAPbBr₃ Perovskite with Reduced Crystal Size. *ACS Energy Lett.* **2018**, *3*, 1458–1466.
- (28) Zheng, K.; Zhu, Q.; Abdellah, M.; Messing, M. E.; Zhang, W.; Generalov, A.; Niu, Y.; Ribaud, L.; Canton, S. E.; Pullerits, T. Exciton Binding Energy and the Nature of Emissive States in Organometal Halide Perovskites. *J. Phys. Chem. Lett.* **2015**, *6*, 2969–2975.
- (29) Yang, Z.; Surrente, A.; Galkowski, K.; Miyata, A.; Portugall, O.; Sutton, R. J.; Haghhighrad, A. A.; Snaith, H. J.; Maude, D. K.; Plochocka, P.; et al. Impact of the Halide Cage on the Electronic Properties of Fully Inorganic Cesium Lead Halide Perovskites. *ACS Energy Lett.* **2017**, *2*, 1621–1627.
- (30) Meulenbergh, R. W.; Lee, J. R. L.; Wolcott, A.; Zhang, J. Z.; Terminello, L. J.; van Buuren, T. Determination of the Exciton Binding Energy in CdSe Quantum Dots. *ACS Nano* **2009**, *3*, 325–330.
- (31) Kagan, C. R.; Murray, C. B.; Nirmal, M.; Bawendi, M. G. Electronic Energy Transfer in Cdse Quantum Dot Solids. *Phys. Rev. Lett.* **1996**, *76*, 1517–1520.
- (32) Thuy, U. T. D.; Thuy, P. T.; Liem, N. Q.; Li, L.; Reiss, P. Comparative Photoluminescence Study of Close-Packed and Colloidal InP/ZnS Quantum Dots. *Appl. Phys. Lett.* **2010**, *96*, 073102.
- (33) Di Stasio, F.; Christodoulou, S.; Huo, N.; Konstantatos, G. Near-Unity Photoluminescence Quantum Yield in CsPbBr₃ Nanocrystal Solid-State Films Via Postsynthesis Treatment with Lead Bromide. *Chem. Mater.* **2017**, *29*, 7663–7667.
- (34) Protesescu, L.; Yakunin, S.; Bodnarchuk, M. I.; Bertolotti, F.; Masciocchi, N.; Guagliardi, A.; Kovalenko, M. V. Monodisperse Formamidinium Lead Bromide Nanocrystals with Bright and Stable Green Photoluminescence. *J. Am. Chem. Soc.* **2016**, *138*, 14202–14205.
- (35) Fu, M.; Tamarat, P.; Trebbia, J.-B.; Bodnarchuk, M. I.; Kovalenko, M. V.; Even, J.; Lounis, B. Unraveling Exciton–phonon Coupling in Individual FAPbI₃ Nanocrystals Emitting Near-infrared Single Photons. *Nat. Commun.* **2018**, *9*, 3318.
- (36) Cordones, A. A.; Leone, S. R. Mechanisms for Charge Trapping in Single Semiconductor Nanocrystals Probed by Fluorescence Blinking. *Chem. Soc. Rev.* **2013**, *42*, 3209–3221.

- (37) Mahler, B.; Spinicelli, P.; Buil, S.; Quelin, X.; Hermier, J.-P.; Dubertret, B. Towards Non-Blinking Colloidal Quantum Dots. *Nat. Mater.* **2008**, *7*, 659–664.
- (38) Zhou, J.; Zhu, M.; Meng, R.; Qin, H.; Peng, X. Ideal CdSe/CdS Core/Shell Nanocrystals Enabled by Entropic Ligands and Their Core Size-, Shell Thickness-, and Ligand-Dependent Photoluminescence Properties. *J. Am. Chem. Soc.* **2017**, *139*, 16556–16567.
- (39) Gibson, N. A.; Koscher, B. A.; Alivisatos, A. P.; Leone, S. R. Excitation Intensity Dependence of Photoluminescence Blinking in CsPbBr₃ Perovskite Nanocrystals. *J. Phys. Chem. C* **2018**, *122*, 12106–12113.
- (40) Seth, S.; Ahmed, T.; Samanta, A. Photoluminescence Flickering and Blinking of Single CsPbBr₃ Perovskite Nanocrystals: Revealing Explicit Carrier Recombination Dynamics. *J. Phys. Chem. Lett.* **2018**, *9*, 7007–7014.
- (41) Swarnkar, A.; Chulliyil, R.; Ravi, V. K.; Irfanullah, M.; Chowdhury, A.; Nag, A. Colloidal CsPbBr₃ Perovskite Nanocrystals: Luminescence Beyond Traditional Quantum Dots. *Angew. Chem., Int. Ed.* **2015**, *54*, 15424–15428.
- (42) Sargent, E. H. Infrared Quantum Dots. *Adv. Mater.* **2005**, *17*, 515–522.
- (43) Buin, A.; Pietsch, P.; Xu, J.; Voznyy, O.; Ip, A. H.; Comin, R.; Sargent, E. H. Materials Processing Routes to Trap-Free Halide Perovskites. *Nano Lett.* **2014**, *14*, 6281–6286.
- (44) Brandt, R. E.; Stevanović, V.; Ginley, D. S.; Buonassisi, T. Identifying Defect-Tolerant Semiconductors with High Minority-Carrier Lifetimes: Beyond Hybrid Lead Halide Perovskites. *MRS Commun.* **2015**, *5*, 265–275.
- (45) Kang, J.; Wang, L.-W. High Defect Tolerance in Lead Halide Perovskite CsPbBr₃. *J. Phys. Chem. Lett.* **2017**, *8*, 489–493.
- (46) Even, J.; Pedesseau, L.; Jancu, J.-M.; Katan, C. Importance of Spin–Orbit Coupling in Hybrid Organic/Inorganic Perovskites for Photovoltaic Applications. *J. Phys. Chem. Lett.* **2013**, *4*, 2999–3005.
- (47) Akkerman, Q. A.; Rainò, G.; Kovalenko, M. V.; Manna, L. Genesis, Challenges and Opportunities for Colloidal Lead Halide Perovskite Nanocrystals. *Nat. Mater.* **2018**, *17*, 394–405.
- (48) Kovalenko, M. V.; Protesescu, L.; Bodnarchuk, M. I. Properties and Potential Optoelectronic Applications of Lead Halide Perovskite Nanocrystals. *Science* **2017**, *358*, 745–750.
- (49) Egger, D. A.; Bera, A.; Cahen, D.; Hodes, G.; Kirchartz, T.; Kronik, L.; Lovrincic, R.; Rappe, A. M.; Reichman, D. R.; Yaffe, O. What Remains Unexplained about the Properties of Halide Perovskites? *Adv. Mater.* **2018**, *30*, 1800691.
- (50) Huang, H.; Bodnarchuk, M. I.; Kershaw, S. V.; Kovalenko, M. V.; Rogach, A. L. Lead Halide Perovskite Nanocrystals in the Research Spotlight: Stability and Defect Tolerance. *ACS Energy Lett.* **2017**, *2*, 2071–2083.
- (51) Kroupa, D. M.; Vörös, M.; Brawand, N. P.; McNichols, B. W.; Miller, E. M.; Gu, J.; Nozik, A. J.; Sellinger, A.; Galli, G.; Beard, M. C. Tuning Colloidal Quantum Dot Band Edge Positions Through Solution-Phase Surface Chemistry Modification. *Nat. Commun.* **2017**, *8*, 15257.
- (52) Li, C.; Lu, X.; Ding, W.; Feng, L.; Gao, Y.; Guo, Z. Formability of ABX₃ (X = F, Cl, Br, I) Halide Perovskites. *Acta Crystallogr., Sect. B: Struct. Sci.* **2008**, *64*, 702–707.
- (53) Ruddlesden, S. N.; Popper, P. New Compounds of the K₂NiF₄ Type. *Acta Crystallogr.* **1957**, *10*, 538–539.
- (54) Saparov, B.; Mitić, D. B. Organic–Inorganic Perovskites: Structural Versatility for Functional Materials Design. *Chem. Rev.* **2016**, *116*, 4558–4596.
- (55) Weidman, M. C.; Goodman, A. J.; Tisdale, W. A. Colloidal Halide Perovskite Nanoplatelets: An Exciting New Class of Semiconductor Nanomaterials. *Chem. Mater.* **2017**, *29*, 5019–5030.
- (56) Reiss, P. ZnSe Based Colloidal Nanocrystals: Synthesis, Shape Control, Core/Shell, Alloy and Doped Systems. *New J. Chem.* **2007**, *31*, 1843–1852.
- (57) Wang, A.; Guo, Y.; Muhammad, F.; Deng, Z. Controlled Synthesis of Lead-Free Cesium Tin Halide Perovskite Cubic Nanocages with High Stability. *Chem. Mater.* **2017**, *29*, 6493–6501.
- (58) Jellicoe, T. C.; Richter, J. M.; Glass, H. F. J.; Tabachnyk, M.; Brady, R.; Dutton, S. E.; Rao, A.; Friend, R. H.; Credgington, D.; Greenham, N. C.; et al. Synthesis and Optical Properties of Lead-Free Cesium Tin Halide Perovskite Nanocrystals. *J. Am. Chem. Soc.* **2016**, *138*, 2941–2944.
- (59) Yang, P.; Liu, G.; Liu, B.; Liu, X.; Lou, Y.; Chen, J.; Zhao, Y. All Inorganic Cs₂CuX₄ (X = Cl, Br, I) Halide Perovskite Quantum Dots with Blue-Green Luminescence. *Chem. Commun.* **2018**, *54*, 11638–11641.
- (60) Regulacio, M. D.; Han, M.-Y. Composition-Tunable Alloyed Semiconductor Nanocrystals. *Acc. Chem. Res.* **2010**, *43*, 621–630.
- (61) Norris, D. J.; Efros, A. L.; Erwin, S. C. Review: Doped Nanocrystals. *Science* **2008**, *319*, 1776–1779.
- (62) Guria, A. K.; Dutta, S. K.; Adhikari, S. D.; Pradhan, N. Doping Mn²⁺ in Lead Halide Perovskite Nanocrystals: Successes and Challenges. *ACS Energy Lett.* **2017**, *2*, 1014–1021.
- (63) Liu, H.; Wu, Z.; Shao, J.; Yao, D.; Gao, H.; Liu, Y.; Yu, W.; Zhang, H.; Yang, B. CsPb_{1-x}Mn_xCl₃ Perovskite Quantum Dots with High Mn Substitution Ratio. *ACS Nano* **2017**, *11*, 2239–2247.
- (64) Arunkumar, P.; Gil, K. H.; Won, S.; Unithrattil, S.; Kim, Y. H.; Kim, H. J.; Im, W. B. Colloidal Organolead Halide Perovskite with a High Mn Solubility Limit: A Step Toward Pb-Free Luminescent Quantum Dots. *J. Phys. Chem. Lett.* **2017**, *8*, 4161–4166.
- (65) Yong, Z. J.; Guo, S. Q.; Ma, J. P.; Zhang, J. Y.; Li, Z. Y.; Chen, Y. M.; Zhang, B. B.; Zhou, Y.; Shu, J.; Gu, J. L.; et al. Doping-Enhanced Short-Range Order of Perovskite Nanocrystals for Near-Unity Violet Luminescence Quantum Yield. *J. Am. Chem. Soc.* **2018**, *140*, 9942–9951.
- (66) Lu, M.; Zhang, X.; Zhang, Y.; Guo, J.; Shen, X.; Yu, W. W.; Rogach, A. L. Simultaneous Strontium Doping and Chlorine Surface Passivation Improve Luminescence Intensity and Stability of CsPbI₃ Nanocrystals Enabling Efficient Light-Emitting Devices. *Adv. Mater.* **2018**, *30*, 1804691.
- (67) Milstein, T. J.; Kroupa, D. M.; Gamelin, D. R. Picosecond Quantum Cutting Generates Photoluminescence Quantum Yields over 100% in Ytterbium-Doped CsPbCl₃ Nanocrystals. *Nano Lett.* **2018**, *18*, 3792–3799.
- (68) Swarnkar, A.; Mir, W. J.; Nag, A. Can B-Site Doping or Alloying Improve Thermal- and Phase-Stability of All-Inorganic CsPbX₃ (X = Cl, Br, I) Perovskites? *ACS Energy Lett.* **2018**, *3*, 286–289.
- (69) Yao, J.; Ge, J.; Han, B.-N.; Wang, K.-H.; Yao, H.-B.; Yu, H.-L.; Li, J.-H.; Zhu, B.-S.; Song, J.; Chen, C.; et al. Ce³⁺-Doping to Modulate Photoluminescence Kinetics for Efficient CsPbBr₃ Nanocrystals Based Light-Emitting Diodes. *J. Am. Chem. Soc.* **2018**, *140*, 3626–3634.
- (70) Liu, F.; Ding, C.; Zhang, Y.; Ripolles, T. S.; Kamisaka, T.; Toyoda, T.; Hayase, S.; Minemoto, T.; Yoshino, K.; Dai, S.; et al. Colloidal Synthesis of Air-Stable Alloyed CsSn_{1-x}Pb_xI₃ Perovskite Nanocrystals for Use in Solar Cells. *J. Am. Chem. Soc.* **2017**, *139*, 16708–16719.
- (71) Zhang, X.; Cao, W.; Wang, W.; Xu, B.; Liu, S.; Dai, H.; Chen, S.; Wang, K.; Sun, X. W. Efficient Light-Emitting Diodes Based on Green Perovskite Nanocrystals with Mixed-Metal Cations. *Nano Energy* **2016**, *30*, 511–516.
- (72) Rivest, J. B.; Jain, P. K. Cation Exchange on the Nanoscale: An Emerging Technique for New Material Synthesis, Device Fabrication, and Chemical Sensing. *Chem. Soc. Rev.* **2013**, *42*, 89–96.
- (73) De Trizio, L.; Manna, L. Forging Colloidal Nanostructures Via Cation Exchange Reactions. *Chem. Rev.* **2016**, *116*, 10852–10887.
- (74) Li, H.; Zanella, M.; Genovese, A.; Povia, M.; Falqui, A.; Giannini, C.; Manna, L. Sequential Cation Exchange in Nanocrystals: Preservation of Crystal Phase and Formation of Metastable Phases. *Nano Lett.* **2011**, *11*, 4964–4970.
- (75) Akkerman, Q. A.; Genovese, A.; George, C.; Prato, M.; Moreels, I.; Casu, A.; Marras, S.; Curcio, A.; Scarpellini, A.; Pellegrino, T.; et al. From Binary Cu₂S to Ternary Cu-In-S and Quaternary Cu-In-Zn-S Nanocrystals with Tunable Composition via Partial Cation Exchange. *ACS Nano* **2015**, *9*, 521–531.

- (76) Van der Stam, W.; Bladt, E.; Rabouw, F. T.; Bals, S.; de Mello Donegá, C. Near-Infrared Emitting CuInSe₂/CuInS₂ Dot Core/Rod Shell Heteronanorods by Sequential Cation Exchange. *ACS Nano* **2015**, *9*, 11430–11438.
- (77) Eames, C.; Frost, J. M.; Barnes, P. R.; O'Regan, B. C.; Walsh, A.; Islam, M. S. Ionic Transport in Hybrid Lead Iodide Perovskite Solar Cells. *Nat. Commun.* **2015**, *6*, 7497.
- (78) Van der Stam, W.; Geuchies, J. J.; Altantzis, T.; Van Den Bos, K. H. W.; Meeldijk, J. D.; Van Aert, S.; Bals, S.; Vanmaekelbergh, D.; De Mello Donegá, C. Highly Emissive Divalent-Ion-Doped Colloidal CsPb_{1-x}M_xBr₃ Perovskite Nanocrystals Through Cation Exchange. *J. Am. Chem. Soc.* **2017**, *139*, 4087–4097.
- (79) Gao, D.; Qiao, B.; Xu, Z.; Song, D.; Song, P.; Liang, Z.; Shen, Z.; Cao, J.; Zhang, J.; Zhao, S. Postsynthetic, Reversible Cation Exchange Between Pb²⁺ and Mn²⁺ in Cesium Lead Chloride Perovskite Nanocrystals. *J. Phys. Chem. C* **2017**, *121*, 20387–20395.
- (80) Xu, W.; Li, F.; Lin, F.; Chen, Y.; Cai, Z.; Wang, Y.; Chen, X. Synthesis of CsPbCl₃-Mn Nanocrystals via Cation Exchange. *Adv. Opt. Mater.* **2017**, *5*, 1700520.
- (81) Tamang, S.; Lincheneau, C.; Hermans, Y.; Jeong, S.; Reiss, P. Chemistry of InP Nanocrystal Syntheses. *Chem. Mater.* **2016**, *28*, 2491–2506.
- (82) Battaglia, D.; Peng, X. Formation of High Quality InP and InAs Nanocrystals in a Noncoordinating Solvent. *Nano Lett.* **2002**, *2*, 1027–1030.
- (83) Ramasamy, P.; Ko, K.-J.; Kang, J.-W.; Lee, J.-S. Two-Step “Seed-Mediated” Synthetic Approach to Colloidal Indium Phosphide Quantum Dots with High-Purity Photo- and Electroluminescence. *Chem. Mater.* **2018**, *30*, 3643–3647.
- (84) Li, L.; Reiss, P. One-Pot Synthesis of Highly Luminescent InP/ZnS Nanocrystals Without Precursor Injection. *J. Am. Chem. Soc.* **2008**, *130*, 11588–11589.
- (85) Park, J. P.; Lee, J.-J.; Kim, S.-W. Highly Luminescent InP/GaP/ZnS QDs Emitting in the Entire Color Range Via a Heating up Process. *Sci. Rep.* **2016**, *6*, 30094.
- (86) Nelson, R. D.; Santra, K.; Wang, Y.; Hadi, A.; Petrich, J. W.; Panthani, M. G. Synthesis and Optical Properties of Ordered-Vacancy Perovskite Cesium Bismuth Halide Nanocrystals. *Chem. Commun.* **2018**, *54*, 3640–3643.
- (87) Hoefler, S. F.; Trimmel, G.; Rath, T. Progress on Lead-Free Metal Halide Perovskites for Photovoltaic Applications: A Review. *Monatsh. Chem.* **2017**, *148*, 795–826.
- (88) Leng, M.; Yang, Y.; Chen, Z.; Gao, W.; Zhang, J.; Niu, G.; Li, D.; Song, H.; Zhang, J.; Jin, S.; et al. Surface Passivation of Bismuth-Based Perovskite Variant Quantum Dots to Achieve Efficient Blue Emission. *Nano Lett.* **2018**, *18*, 6076–6083.
- (89) Yang, B.; Chen, J.; Hong, F.; Mao, X.; Zheng, K.; Yang, S.; Li, Y.; Pullerits, T.; Deng, W.; Han, K. Lead-Free, Air-Stable All-Inorganic Cesium Bismuth Halide Perovskite Nanocrystals. *Angew. Chem., Int. Ed.* **2017**, *56*, 12471–12475.
- (90) Zhang, J.; Yang, Y.; Deng, H.; Farooq, U.; Yang, X.; Khan, J.; Tang, J.; Song, H. High Quantum Yield Blue Emission from Lead-Free Inorganic Antimony Halide Perovskite Colloidal Quantum Dots. *ACS Nano* **2017**, *11*, 9294–9302.
- (91) Wang, A.; Yan, X.; Zhang, M.; Sun, S.; Yang, M.; Shen, W.; Pan, X.; Wang, P.; Deng, Z. Controlled Synthesis of Lead-Free and Stable Perovskite Derivative Cs₂SnI₆ Nanocrystals via a Facile Hot-Injection Process. *Chem. Mater.* **2016**, *28*, 8132–8140.
- (92) Dolzhenkov, D. S.; Wang, C.; Xu, Y.; Kanatzidis, M. G.; Weiss, E. A. Ligand-Free, Quantum-Confined Cs₂SnI₆ Perovskite Nanocrystals. *Chem. Mater.* **2017**, *29*, 7901–7907.
- (93) Amit, Y.; Eshet, H.; Faust, A.; Patlola, A.; Rabani, E.; Banin, U.; Frenkel, A. I. Unraveling the Impurity Location and Binding in Heavily Doped Semiconductor Nanocrystals: The Case of Cu in InAs Nanocrystals. *J. Phys. Chem. C* **2013**, *117*, 13688–13696.
- (94) Mocatta, D.; Cohen, G.; Schattner, J.; Millo, O.; Rabani, E.; Banin, U. Heavily Doped Semiconductor Nanocrystal Quantum Dots. *Science* **2011**, *332*, 77–81.
- (95) Sahu, A.; Kang, M. S.; Kompch, A.; Notthoff, C.; Wills, A. W.; Deng, D.; Winterer, M.; Frisbie, C. D.; Norris, D. J. Electronic Impurity Doping in CdSe Nanocrystals. *Nano Lett.* **2012**, *12*, 2587–2594.
- (96) Pan, G.; Bai, X.; Yang, D.; Chen, X.; Jing, P.; Qu, S.; Zhang, L.; Zhou, D.; Zhu, J.; Xu, W.; et al. Doping Lanthanide into Perovskite Nanocrystals: Highly Improved and Expanded Optical Properties. *Nano Lett.* **2017**, *17*, 8005–8011.
- (97) Zhou, D.; Liu, D.; Pan, G.; Chen, X.; Li, D.; Xu, W.; Bai, X.; Song, H. Cerium and Ytterbium Codoped Halide Perovskite Quantum Dots: A Novel and Efficient Downconverter for Improving the Performance of Silicon Solar Cells. *Adv. Mater.* **2017**, *29*, 1704149.
- (98) Hu, Q.; Li, Z.; Tan, Z.; Song, H.; Ge, C.; Niu, G.; Han, J.; Tang, J. Rare Earth Ion-Doped CsPbBr₃ Nanocrystals. *Adv. Opt. Mater.* **2018**, *6*, 1700864.
- (99) Begum, R.; Parida, M. R.; Abdelhady, A. L.; Murali, B.; Alyami, N. M.; Ahmed, G. H.; Hedhili, M. N.; Bakr, O. M.; Mohammed, O. F. Engineering Interfacial Charge Transfer in CsPbBr₃ Perovskite Nanocrystals by Heterovalent Doping. *J. Am. Chem. Soc.* **2017**, *139*, 731–737.
- (100) Liu, M.; Zhong, G.; Yin, Y.; Miao, J.; Li, K.; Wang, C.; Xu, X.; Shen, C.; Meng, H. Aluminum-Doped Cesium Lead Bromide Perovskite Nanocrystals with Stable Blue Photoluminescence Used for Display Backlight. *Adv. Sci.* **2017**, *4*, 1700335.
- (101) Wang, H.-C.; Wang, W.; Tang, A.-C.; Tsai, H.-Y.; Bao, Z.; Ihara, T.; Yarita, N.; Tahara, H.; Kanemitsu, Y.; Chen, S.; et al. High-Performance CsPb_{1-x}Sn_xBr₃ Perovskite Quantum Dots for Light-Emitting Diodes. *Angew. Chem.* **2017**, *129*, 13838–13842.
- (102) Aldakov, D.; Lefrançois, A.; Reiss, P. Ternary and Quaternary Metal Chalcogenide Nanocrystals: Synthesis, Properties and Applications. *J. Mater. Chem. C* **2013**, *1*, 3756–3776.
- (103) Zunger, A.; Zhang, S. B.; Su-Huai, W. Revisiting the Defect Physics in CuInSe₂ and CuGaSe₂. *Conf. Rec. 26. IEEE Photovolt. Spec. Conf.* **1997**, 313–318.
- (104) Reiss, P.; Li, L.; Daou, T. J.; Texier-Nogues, I. Fluorescent Nanoparticles, Method for Preparing Same, and Application Thereof in Biological Marking. FR0857497 (2008)/US 2012/0061627.
- (105) Li, L.; Daou, T. J.; Texier, I.; Thi, T.; Chi, K.; Liem, N. Q.; Reiss, P. Highly Luminescent CuInS₂/ZnS Core/Shell Nanocrystals: Cadmium-Free Quantum Dots for In Vivo Imaging. *Chem. Mater.* **2009**, *21*, 2422–2429.
- (106) Tran, T. K. T.; Le, Q. P.; Nguyen, Q. L.; Li, L.; Reiss, P. Time-Resolved Photoluminescence Study of CuInS₂/ZnS Nanocrystals. *Adv. Nat. Sci.: Nanosci. Nanotechnol.* **2010**, *1*, 025007.
- (107) Zang, H.; Li, H.; Makarov, N. S.; Velizhanin, K. A.; Wu, K.; Park, Y.-S.; Klimov, V. I. Thick-Shell CuInS₂/ZnS Quantum Dots with Suppressed “Blinking” and Narrow Single-Particle Emission Line Widths. *Nano Lett.* **2017**, *17*, 1787–1795.
- (108) Zhong, H.; Lo, S. S.; Mirkovic, T.; Li, Y.; Ding, Y.; Li, Y.; Scholes, G. D. Noninjection Gram-Scale Synthesis of Monodisperse Pyramidal CuInS₂ Nanocrystals and Their Size-Dependent Properties. *ACS Nano* **2010**, *4*, 5253–5262.
- (109) Zhong, H.; Wang, Z.; Bovero, E.; Lu, Z.; van Veggel, F. C. J. M.; Scholes, G. D. Colloidal CuInSe₂ Nanocrystals in the Quantum Confinement Regime: Synthesis, Optical Properties, and Electrochromism. *J. Phys. Chem. C* **2011**, *115*, 12396–12402.
- (110) Gromova, M.; Lefrançois, A.; Vaure, L.; Agnese, F.; Aldakov, D.; Maurice, A.; Djurado, D.; Lebrun, C.; de Geyer, A.; Schüllli, T. U.; et al. Growth Mechanism and Surface State of CuInS₂ Nanocrystals Synthesized with Dodecanethiol. *J. Am. Chem. Soc.* **2017**, *139*, 15748–15759.
- (111) Lefrançois, A.; Luszczynska, B.; Pépin-Donat, B.; Lombard, C.; Bouthinon, B.; Verilhac, J.-M.; Gromova, M.; Faure-Vincent, J.; Pouget, S.; Chandezon, F.; et al. Enhanced Charge Separation in Ternary P3HT/PCBM/CuInS₂ Nanocrystals Hybrid Solar Cells. *Sci. Rep.* **2015**, *5*, 7768.
- (112) Aldakov, D.; Sajjad, M. T.; Ivanova, V.; Bansal, A. K.; Park, J.; Reiss, P.; Samuel, I. D. W. Mercaptophosphonic Acids as Efficient

Linkers in Quantum Dot Sensitized Solar Cells. *J. Mater. Chem. A* **2015**, *3*, 19050–19060.

(113) Park, J.; Sajjad, M. T.; Jouneau, P.-H.; Ruseckas, A.; Faure-Vincent, J.; Samuel, I. D. W.; Reiss, P.; Aldakov, D. Efficient Eco-Friendly Inverted Quantum Dot Sensitized Solar Cells. *J. Mater. Chem. A* **2016**, *4*, 827–837.

(114) Sajjad, M. T.; Park, J.; Gaboriau, D.; Harwell, J. R.; Odobel, F.; Reiss, P.; Samuel, I. D. W.; Aldakov, D. CuSCN Nanowires as Electrodes for p-Type Quantum Dot Sensitized Solar Cells: Charge Transfer Dynamics and Alumina Passivation. *J. Phys. Chem. C* **2018**, *122*, 5161–5170.

(115) Luszczynska, B.; Szymanski, M. Z.; Verilhac, J.-M.; Reiss, P.; Djurado, D. Improved External Quantum Efficiency of Solution-Processed P3HT:60PCBM Photodetectors by the Addition of Cu–In–Se Nanocrystals. *Org. Electron.* **2013**, *14*, 3206–3212.

(116) Sandroni, M.; Gueret, R.; Wegner, K. D.; Reiss, P.; Fortage, J.; Aldakov, D.; Collomb, M.-N. Cadmium-Free CuInS₂/ZnS Quantum Dots as Efficient and Robust Photosensitizers in Combination with a Molecular Catalyst for Visible Light-Driven H₂ Production in Water. *Energy Environ. Sci.* **2018**, *11*, 1752–1761.

(117) Sandroni, M.; Wegner, K. D.; Aldakov, D.; Reiss, P. Prospects of Chalcopyrite-Type Nanocrystals for Energy Applications. *ACS Energy Lett.* **2017**, *2*, 1076–1088.

(118) <https://ubiqd.com> (accessed Jan. 16, 2019).

(119) Coughlan, C.; Ibáñez, M.; Dobrozhan, O.; Singh, A.; Cabot, A.; Ryan, K. M. Compound Copper Chalcogenide Nanocrystals. *Chem. Rev.* **2017**, *117*, 5865–6109.

(120) Gabka, G.; Bujak, P.; Gryszel, M.; Ostrowski, A.; Malinowska, K.; Zukowska, G. Z.; Agnese, F.; Pron, A.; Reiss, P. Synthesis and Surface Chemistry of High Quality Wurtzite and Kesterite Cu₂ZnSnS₄ Nanocrystals Using Tin(II) 2-Ethylhexanoate as a New Tin Source. *Chem. Commun.* **2015**, *51*, 12985–12988.

(121) Bekenstein, Y.; Dahl, J. C.; Huang, J.; Osowiecki, W. T.; Swabeck, J. K.; Chan, E. M.; Yang, P.; Alivisatos, A. P. The Making and Breaking of Lead-Free Double Perovskite Nanocrystals of Cesium Silver-Bismuth Halide Compositions. *Nano Lett.* **2018**, *18*, 3502–3508.

(122) Creutz, S. E.; Crites, E. N.; De Siena, M. C.; Gamelin, D. R. Colloidal Nanocrystals of Lead-Free Double-Perovskite (Elpasolite) Semiconductors: Synthesis and Anion Exchange to Access New Materials. *Nano Lett.* **2018**, *18*, 1118–1123.

(123) Yang, B.; Chen, J.; Yang, S.; Hong, F.; Sun, L.; Han, P.; Pullerits, T.; Deng, W.; Han, K. Lead-Free Silver-Bismuth Halide Double Perovskite Nanocrystals. *Angew. Chem., Int. Ed.* **2018**, *57*, 5359–5363.

(124) Zhou, L.; Xu, Y.-F.; Chen, B.-X.; Kuang, D.-B.; Su, C.-Y. Synthesis and Photocatalytic Application of Stable Lead-Free Cs₂AgBiBr₆ Perovskite Nanocrystals. *Small* **2018**, *14*, 1703762.

(125) Locardi, F.; Cirignano, M.; Baranov, D.; Dang, Z.; Prato, M.; Drago, F.; Ferretti, M.; Pinchetti, V.; Fanciulli, M.; Brovelli, S.; et al. Colloidal Synthesis of Double Perovskite Cs₂AgInCl₆ and Mn-Doped Cs₂AgInCl₆ Nanocrystals. *J. Am. Chem. Soc.* **2018**, *140*, 12989–12995.

(126) Giustino, F.; Snaith, H. J. Toward Lead-Free Perovskite Solar Cells. *ACS Energy Lett.* **2016**, *1*, 1233–1240.

(127) Chakraborty, S.; Xie, W.; Mathews, N.; Sherburne, M.; Ahuja, R.; Asta, M.; Mhaisalkar, S. G. Rational Design: A High-Throughput Computational Screening and Experimental Validation Methodology for Lead-Free and Emergent Hybrid Perovskites. *ACS Energy Lett.* **2017**, *2*, 837–845.

(128) Filip, M. R.; Giustino, F. The Geometric Blueprint of Perovskites. *Proc. Natl. Acad. Sci. U. S. A.* **2018**, *115*, 5397–5402.

(129) Chen, S.; Hou, Y.; Chen, H.; Tang, X.; Langner, S.; Li, N.; Stubhan, T.; Levchuk, I.; Gu, E.; Osvet, A.; et al. Exploring the Stability of Novel Wide Bandgap Perovskites by a Robot Based High Throughput Approach. *Adv. Energy Mater.* **2018**, *8*, 1701543.

(130) Lignos, I.; Stavakis, S.; Nedelcu, G.; Protesescu, L.; DeMello, A. J.; Kovalenko, M. V. Synthesis of Cesium Lead Halide Perovskite

Nanocrystals in a Droplet-Based Microfluidic Platform: Fast Parametric Space Mapping. *Nano Lett.* **2016**, *16*, 1869–1877.

(131) Zhang, X.; Wang, C.; Zhang, Y.; Zhang, X.; Wang, S.; Lu, M.; Cui, H.; Kershaw, S. V.; Yu, W. W.; Rogach, A. L. Bright Orange Electroluminescence from Lead-Free Two-Dimensional Perovskites. *ACS Energy Lett.* **2019**, *4*, 242–248.

(132) Bhaumik, S.; Veldhuis, S. A.; Ng, Y. F.; Li, M.; Muduli, S. K.; Sum, T. C.; Damodaran, B.; Mhaisalkar, S.; Mathews, N. Highly Stable, Luminescent Core–Shell Type Methylammonium–octylammonium Lead Bromide Layered Perovskite Nanoparticles. *Chem. Commun.* **2016**, *52*, 7118–7121.

(133) Wang, S.; Bi, C.; Yuan, J.; Zhang, L.; Tian, J. Original Core–Shell Structure of Cubic CsPbBr₃@Amorphous CsPbBr_x Perovskite Quantum Dots with a High Blue Photoluminescence Quantum Yield of over 80%. *ACS Energy Lett.* **2018**, *3*, 245–251.

(134) Geng, C.; Xu, S.; Zhong, H.; Rogach, A. L.; Bi, W. Aqueous Synthesis of Methylammonium Lead Halide Perovskite Nanocrystals. *Angew. Chem., Int. Ed.* **2018**, *57*, 9650–9654.

(135) Huang, H.; Chen, B.; Wang, Z.; Hung, T. F.; Susha, A. S.; Zhong, H.; Rogach, A. L. Water Resistant CsPbX₃ Nanocrystals Coated with Polyhedral Oligomeric Silsesquioxane and Their Use as Solid State Luminophores in All-Perovskite White Light-Emitting Devices. *Chem. Sci.* **2016**, *7*, 5699–5703.

(136) Erwin, S. C.; Zu, L. J.; Haftel, M. I.; Efron, A. L.; Kennedy, T. A.; Norris, D. J. Doping Semiconductor Nanocrystals. *Nature* **2005**, *436*, 91–94.

(137) Tan, Z.; Li, J.; Zhang, C.; Li, Z.; Hu, Q.; Xiao, Z.; Kamiya, T.; Hosono, H.; Niu, G.; Lifshitz, E.; et al. Highly Efficient Blue-Emitting Bi-Doped Cs₂SnCl₆ Perovskite Variant: Photoluminescence Induced by Impurity Doping. *Adv. Funct. Mater.* **2018**, *28*, 1801131.

(138) Shao, H.; Bai, X.; Cui, H.; Pan, G.; Jing, P.; Qu, S.; Zhu, J.; Zhai, Y.; Dong, B.; Song, H. White Light Emission in Bi³⁺/Mn²⁺ Ion Co-Doped CsPbCl₃ Perovskite Nanocrystals. *Nanoscale* **2018**, *10*, 1023–1029.

(139) Filip, M. R.; Eperon, G. E.; Snaith, H. J.; Giustino, F. Steric Engineering of Metal-halide Perovskites with Tunable Optical Band Gaps. *Nat. Commun.* **2014**, *5*, 5757.